UNSTEADY FLOW IN A SMOOTH PIPE AFTER

INSTANTANEOUS OPENING OF A DOWNSTREAM VALVE

Part III. Mean Flow Characteristics—Pressure and Boundary Shear

A THESIS

Presented to

the Faculty of the Graduate Division

Georgia Institute of Technology

In Partial Fulfillment

of the Requirements for the Degree

Master of Science in Civil Engineering

By

John Edwin Roller

June 1956

UNSTEADY FLOW IN A SMOOTH PIPE AFTER

INSTANTANEOUS OPENING OF A DOWNSTREAM VALVE

Part III. Mean Flow Characteristics—Pressure and Boundary Shear

Approved:

Date Approved: May 29, 1956

ACKNOWLEDGMENTS

TABLE OF CONTENTS

Pressure transducer data
Film strip data

One-dimensional equation of motion
Method of investigation
Interpretation of results

LIST OF FIGURES

LIST OF TABLES

SUMMARY

An experimental study was performed in order to determine the mean

flow characteristics in a pipe during flow establishment. The smooth,

straight, circular pipe was horizontally aligned. The upstream extremity

of this pipe was a well-rounded inlet which was located in a large

reservoir. The downstream extremity of this pipe was unobstructed so

that a liquid jet was formed in the atmosphere downstream from the pipe

outlet. Velocity-time data were obtained from a motion picture record

of the jet. Pressure-time data were obtained at selected points along

the pipe. These data were recorded by sending the output signals of

pressure transducers through an oscillograph.

The experiments were performed with a systematic variation of the

independent dimensionless variables. These independent dimensionless

variables were pipe length to pipe diameter ratio L/D and an inertial

reaction to viscous shear force ratio $gh_o D^3/L\nu^2$. h_o is the piezometric

head in the reservoir and ν is the kinematic viscosity of the fluid.

The value of L/D was established at 95, 190, 285, 380, and 475. The

value of $gh_o D^3/L\nu^2$ was established at $6(10^6)$, $12(10^6)$, $18(10^6)$, $24(10^6)$,

and $30(10^6)$. Thus the total number of experimental runs was twenty-five.

In this study only the boundary shear characteristics of unsteady

flow are investigated. Prior to release of the downstream valve, the

fluid is at rest within the pipe. For a short time interval following

the valve opening, the flow is laminar throughout the pipe. At a later

time, the flow becomes unstable, which results in the formation of a spot
or region of turbulence. Still later, more turbulence spots are formed
and these regions of turbulence are enlarged until the flow is turbulent
throughout the entire length of the pipe. The objectives of the study
are (1) to determine empirically the boundary shear forces in both
laminar and turbulent unsteady flow, utilizing experimental velocity
and pressure data; and (2) to compare the results with steady-flow
relationships.

Supplementary analysis was required in order to determine the
mean velocity in the pipe from the motion picture record of the jet. As
the result of the action of shear forces, the velocity distribution is
non-uniform. Consequently the jet issuing from the pipe outlet had
greater linear momentum than if the velocity distribution were uniform.
Thus the problem was to determine the non-uniformity of the velocity
distribution in order to relate the observed velocity to the mean
velocity. During the laminar flow, a solution of the Navier-Stokes
equations was utilized in which the experimentally determined piezo-
metric head-time data were introduced. Since the analytical solution
does not cover the complete temporal range of laminar flow, an empirical
method based upon observed velocity data was utilized to extrapolate
the analytical solution. For turbulent flow, the velocity was assumed
to have a distribution based upon the seventh-root law of velocity
distribution.

Unsteady laminar and turbulent boundary shear, as reflected in
the value of the Darcy-Weisbach resistance coefficient f may be

empirically determined by utilization of the corrected experimental data
and the one-dimensional equation of motion. All empirical values are
compared with steady-flow relations by utilization of a ratio of f_{steady}
and $f_{unsteady}$, thus eliminating the Reynolds number from consideration.
In addition, an analytical analysis of laminar shear was utilized for
comparison with experimental data.

Unsteady shear results are presented in graphical and tabular
form.

Significant results obtained from the study are: (1) The one-
dimensional solution of the Navier-Stokes equations is an excellent in-
vestigative approach for determining the flow characteristics of un-
steady laminar flow in a pipe. (2) A single parameter representation
of velocity profile characteristics is inadequate for singular correla-
tion of laminar shear for all flow conditions. Thus there is no unique
velocity profile relation for unsteady laminar flow. Laminar shear at
any stage of flow development is dependent upon initial conditions and
intervening flow conditions. (3) The experimental turbulent shear data
are indicative of a qualitative effect of unsteadiness on turbulent
shear. An increase in f is observed with fluid deceleration and a
corresponding decrease is observed with fluid acceleration.

UNSTEADY FLOW IN A SMOOTH PIPE AFTER

INSTANTANEOUS OPENING OF A DOWNSTREAM VALVE

Part III. Mean Flow Characteristics--Pressure and Boundary Shear

INTRODUCTION

A study of the mechanics of flow establishment in a pipe was per-
formed in the Hydraulics Laboratory, School of Civil Engineering, Georgia
Institute of Technology. The experiments were performed with a smooth,
straight, circular pipe which was horizontally aligned. The upstream
extremity of the pipe was a well-rounded inlet which was located in a
large reservoir. The downstream extremity of the pipe was unobstructed
so that a liquid jet was formed in the atmosphere downstream from the
pipe. The flow was established by rapid (effectively instantaneous)
release of a disk valve placed against the square-edged downstream end
of the pipe. Velocity-time data were obtained from a motion-picture
record of the jet. Pressure-time data were obtained at selected sta-
tions along the pipe. These data were recorded as an oscillograph
record of the output signals of pressure transducers.

The experiments were performed with a systematic variation of the
independent dimensionless variables in the equations:

$$\frac{V}{\sqrt{2gh_o}} = \phi \left[\frac{t \sqrt{gh_o}}{L} , \frac{L}{D} , \frac{gh_o D^3}{L \nu^2} \right]$$

and

$$\frac{h}{h_o} = \phi \left[\frac{t \sqrt{gh_o}}{L} , \frac{L}{D} , \frac{gh_o D^3}{L\mathcal{V}2} \right]$$

The letter symbols are defined as follows:

D   - inside diameter of pipe;

g   - acceleration of gravity;

h   - piezometric head in the pipe;

h_o - piezometric head in the reservoir;

L   - length of pipe;

$\mathcal{V}$ - kinematic viscosity of the fluid;

t   - time since valve opening; and,

V   - mean velocity in the pipe.

Results obtained from ten experimental runs (Runs 20-29, inclusive) are reported in this paper. The value of L/D was 380.3 in Runs 20-24 and was 475.3 in Runs 25-29. The other externally controlled variable $gh_o D^3/L\mathcal{V}^2$ was established at values of $6(10^6)$, $12(10^6)$, $18(10^6)$, $24(10^6)$, and $30(10^6)$.

In this study only the boundary shear characteristics of unsteady flow are investigated. Prior to release of the downstream valve, the fluid is at rest within the pipe. For a short time interval following the valve opening, the flow is laminar throughout the pipe. At a later time, the flow becomes unstable, which results in the formation of a spot or region of turbulence. Still later, more turbulence spots are formed and these regions of turbulence are enlarged until the flow is

turbulent throughout the entire length of the pipe. The detailed objectives of this study are (1) to determine empirically the boundary shear forces in both laminar and turbulent unsteady flow, utilizing experimental velocity and pressure data; and (2) to compare the results with steady-flow relationships.

EXPERIMENTAL EQUIPMENT AND TECHNIQUE

Figure 1 is a schematic drawing of the equipment. The description of the equipment components is presented from the upstream section to the downstream.

The reservoir was a sealed cylindrical steel tank with a diameter of 42 inches. The air pressure in the reservoir above the water was controlled to any desired level by means of an air overflow line. The air overflow was allowed to bubble into the bottom of a standpipe. Thus by controlling the water level in the standpipe, the air pressure in the reservoir could be maintained so as to obtain the desired magnitude of the reservoir piezometric head h_o. No make-up water was added to the reservoir during a run and no run was made without allowing the reservoir to be quiescent for at least four hours. Since the tank cross section was large and the volume of air above the water was large, the piezometric head change was negligible during the short time required for a run. With this arrangement, the value of $gh_o D^3/L \mathcal{V}^2$ was determined within an estimated accuracy of $\pm 0.4\%$ and the magnitude was controlled within $\pm 1.0\%$ of the desired value.

The pipe leading from the reservoir consisted of coupled sections of extra-heavy smooth brass pipe. In order to easily and systematically

vary the pipe length, five sections approximately 95 diameters in length were machined and fitted to insure smooth junctures and proper alignment when forced into the machined-brass sleeve couplings. An adjustable mount on each pipe section allowed the pipe to be aligned along a straight horizontal axis.

The extruded brass pipe proved to be extremely uniform in diameter. Micrometer measurements were taken on orthogonal diameters at each end section. The mean diameter of these twenty measurements was 0.544 inch with all readings being within $\pm$ 0.001 inch of this value. The average diameter of each pipe section was also checked by weighing the volume of water that could be placed in each section.

The rounded pipe inlet was located in the reservoir. The inlet piece was attached to the first pipe section by a slip-fit of close tolerance similar to the sleeve coupling. The machined brass inlet piece was made with a radius of rounding equal to 1.13 pipe diameters. A band of sand roughness approximately 1/8-inch wide was cemented to the inlet piece slightly upstream from the tangent point of the inlet roundness. The sand gradation used was that which passed the No. 100 screen but which was retained on the No. 200 screen.

Wall piezometer holes were placed 1/2-inch from the downstream end of each pipe section. Four piezometer openings were drilled on orthogonal diameters with a No. 45 drill. The holes were rigidly inspected and any burrs caused by drilling were carefully removed. The four piezometer openings were connected by a piezometer ring which was machined in the pipe sleeve coupling.

Pressure-time measurements were obtained by means of pressure transducers, the signal of which was electrically amplified and recorded. These differential pressure transducers were mounted on a transducer collar so that the water passage from the pressure transducer to the piezometer ring was large in cross section and short in length. The pressure transducers were the unbonded-resistance-wire type. The transducer impulses were amplified and recorded on an oscillograph. The oscillograph contained an independent timing mechanism so that the oscillograph record consisted of the time record as well as the output record of the two pressure transducers. Due to the cost of the transducers and the recording equipment, only two transducers with a two-channel recorder were utilized. Runs with four and five pipe sections (Runs 20-29, inclusive), were duplicated in order to obtain pressure-time records at all piezometer stations.

In order to simplify the boundary conditions associated with the flow establishment, a downstream valve was visualized which could be instantaneously opened and which in the opening process would not influence the resulting fluid motion. The physical requirements of such a valve are (a) in a negligible time after valve release the pressure at the pipe outlet must drop from the reservoir piezometric pressure to atmospheric pressure, and (b) the valve body must be moved in the same direction and with a faster motion than the fluid particles issuing from the pipe outlet. The type of valve selected was a flat disk; which was positioned flush against the downstream end of the pipe. The force of a stressed tension spring was utilized to rapidly remove the valve disk away from the oncoming fluid.

Velocity determinations were made from individual frames of a
35 mm motion picture camera record of the jet. The camera was positioned
on a line which was perpendicular to the vertical plane of the jet. The
exposure time for each frame was 0.0015 second. The camera was run at a
speed of approximately 36 frames per second. Rear lighting was used in
order to eliminate jet shadow.

A single unit frame was constructed as a mounting base for the rear-
light source, a time clock, and coordinate grid scales. A distinct rear-
lighted clock image was recorded in each motion picture frame from which
time could be determined to the nearest 0.001 second. A horizontal and
a vertical grid scale were also photographed. These scales were posi-
tioned in the plane of the jet to avoid parallax.

TRANSFORMATION OF DATA INTO A FORM SUITABLE FOR ANALYSIS

With this experimental equipment, the time dependent data was avail-
able in the form of a 35 mm motion picture film strip of the jet and the
oscillograph records from the pressure transducer circuit. The reduction
of the pressure data into a useable from was straight forward. The reduc-
tion of the film strip data into a useable form was complex. In order to
explain the process of data transformation, the data of Run 29 is used
throughout the following description. For Run 29 all five pipe sections
were utilized, that is, the value of L/D was 475. The other independent
variable $gh_0D^3/L\mathcal{V}^2$ was established at the value $30(10^6)$.

Pressure transducer data.---In each run the pressure data as recorded by
the oscillograph was replotted in the form of dimensionless piezometric

head ratio h/h_o as a function of dimensionless time $t\sqrt{gh_o}/L$. Since there was a linear relationship between the deflection of the writing stylus and the piezometric head change, values of h/h_o were determined from scaled-distance ratios. The value of time t was measured from the instant of valve opening. The very rapid change in piezometric head h from the initial value h_o at the instant the valve was opened could be easily discerned on the oscillograph record. Time was measured from this point on the record by the pips of the independent timing stylus. Figure 2 is a plot of h/h_o as a function of t $\sqrt{gh_o}/L$ for Run 29. The position of measurement is given by the dimensionless distance from the inlet x/D. Runs 29 and 29a were duplicate runs in order to obtain pressure measurements at four stations with the two pressure transducers. The pressure at the outlet, x/D = 475, is zero for t > 0.

Film strip data.—Six frames of the film strip of Run 29 are shown on Fig. 3.

Two assumptions were employed to determine fluid velocity from the photographically recorded jet. First, air resistance was considered negligible. Second, the jet was considered to be a succession of fluid masses comprised of individual fluid particles each having the velocity characteristics of this larger group. If the velocity characteristics of the individual particles of a fluid mass are identical, the motion can be completely described by the motion of the mass center of that fluid mass.

Utilizing the two preceding assumptions, a jet discharging freely into the atmosphere is acted upon by the acceleration of gravity alone.

The horizontal component of the velocity is constant throughout the free fall. Since the pipe is horizontal, this constant horizontal component is the velocity of the fluid mass as that fluid mass passed the outlet. The free fall equations are

$$t' = \sqrt{-\frac{2y'}{g}}$$

and

$$V' = x'/t'$$

in which t' is the elapsed time since the fluid mass passed the pipe outlet, x' and y' are the coordinates of the fluid mass measured from the centerline of the pipe outlet, and V' is designated as the observed velocity. The time recorded on the clock in each film strip frame is designated as T for which the zero value is the valve opening time. Hence the time interval t between the time of valve opening and the time that the fluid mass passed the outlet is $t = T - t'$. Thus by observing the x' and y' coordinates and the clock times from the frames of the film strip, the values V' and t can be computed. On Fig. 4 the dimensionless observed velocity $V'/\sqrt{2gh_o}$ is plotted as a function of $t\sqrt{gh_o}/L$.

The magnitude of the error involved in assuming negligible air resistance can be determined by observing the same fluid mass on successive film strip frames. The $V' - t$ relationships determined from x' and T values with the value of y' of -0.5 ft and -2.50 ft were identical, indicating negligible air resistance.

The correctness of the assumption that the jet can be visualized as a series of individual fluid masses is confirmed by the appearance of the jet (Fig. 3). In all the photographs, slugs of fluid appear to be forming in the jet. A logical explanation of why the jet can be considered to be a series of fluid masses is as follows. During the time the fluid is in the pipe, the external force of boundary shear acts on the fluid at the junction of the fluid and pipe wall. This boundary shear force results in a system of internal shear forces within the fluid and results in a radial variation of linear momentum with the fluid particles close to the wall having a momentum deficiency. As the fluid issues from the pipe into the atmosphere, the external boundary shear force is decreased to zero. However the internal shear forces are reduced to zero only if the linear momentum is constant in a cross section. The internal shear forces persist until the jet has constant linear momentum in the cross section. Thus the internal shear forces are the implement for effecting the radial transfer of linear momentum. The result of this process is a jet cross section having uniform linear momentum which is, of course, the assumption utilized in determining the observed velocity V'.

However the observed velocity V' is not the mean velocity V of the pipe flow. Because of the boundary shear force between the fluid and the pipe wall the velocity distribution is not uniform within the pipe. Thus the fluid upon leaving the pipe has a greater linear momentum than if the velocity of all particles were equal to the mean velocity V. Since the linear momentum is constant in a fluid mass after this fluid mass leaves the pipe, the fluid mass attains a velocity V' which is

greater than V. The two velocities are related by the relationship $V = V'/C_m$ in which C_m is the momentum correction coefficient. C_m is a function only of velocity distribution and is defined by the relationship $C_m = (1/A) \int_A (v/V)^2 \, dA$ in which v is the point velocity and A is the cross sectional area of the pipe. Therefore in order to quantitatively utilize the data of Fig. 4 in a study of pipe flow, the velocity distribution had to be determined as a function of time.

The velocity distribution or specifically the value of C_m in unsteady laminar flow was determined by a combination of theoretical analysis and empirical results.

A solution of the Navier-Stokes equations was obtained in which the experimentally determined piezometric head-time data were introduced. If the pipe flow is one-dimensional, that is, the total velocity is axial, two of Navier-Stokes equations are indicative that (a) the piezometric head is constant in a fluid cross section which is normal to the flow and (b) the axial piezometric pressure gradient $\partial p^*/\partial x$ is only a function of time. The remaining equation is

$$\frac{\partial v}{\partial t} = \nu \left[\frac{\partial^2 v}{\partial r^2} + \frac{1}{r} \frac{\partial v}{\partial r} \right] - \frac{1}{\rho} \frac{\partial p^*}{\partial x} \tag{1}$$

in which v is the point velocity and ρ is the mass density. The boundary conditions are that the velocity v is zero at the boundary and that the velocity gradient $\partial v/\partial r$ is zero at the pipe centerline. The initial condition is that the velocity v is zero when time t is zero.

The analogous equation with analogous boundary and initial conditions has been solved for temperature distribution in a cylindrical

rod[1]. The solution for the pipe flow problem is

$$v = \frac{2}{\rho} \sum_{n=1}^{\infty} \frac{J_0(a_n \beta)}{a_n J_1(a_n)} e^{-a_n^2 \alpha} \int_0^t g(\tau) e^{\frac{a_n^2 \nu \tau}{r_0^2}} d\tau \qquad (2)$$

The various terms are as follows: J_0 and J_1 are Bessel functions of the first kind of orders zero and one, respectively; the positive numbers a_n are the zero roots of J_0; r_0 is the value of the radius r at the pipe wall; β is the dimensionless radial coordinate r/r_0; τ is a dummy variable of integration; $g(\tau)$ is $-\partial p^*/\partial x$; and α is $\nu t/r_0^2$.

In order to apply Eq. (2) in the analysis of the experimental results, the existence and location of a one-dimensional laminar flow region must be determined and, then, the time variation of the piezometric pressure gradient $\partial p^*/\partial x$ in this region must be determined from the pressure-time data of Fig. 2.

A physical interpretation of the pressure-time data (Fig. 2) is requisite to locating a laminar flow region. Since the fluid starts from rest, the flow is laminar in the entire pipe during the initial period after the downstream valve is opened. The first external indication that this flow regime has changed is the sharp pressure rises at the piezometers. For example, as shown on Fig. 2, the first of these sharp pressure rises occurred at the location x/D of 189 at the time $t\sqrt{gh_0}/L$ of 0.616. The interpretation of these pressure rises is that an interface

[1]"Fourier Transforms," by Ian N. Sneddon, McGraw-Hill Book Co., Inc., New York, N. Y., 1951, p. 202.

between laminar flow and turbulent flow is passing the piezometer at that time. The reason for the rapid change is that the mean kinetic energy of the cross section is greater in the laminar flow than in the turbulent flow even though the mean velocity V is identical on both sides of the interface. The difference in these kinetic energies is due to the more uniform velocity distribution of turbulent flow. Thus at x/D of 189 the flow was laminar prior to $t\sqrt{gh_0}/L$ of 0.616 and was turbulent during the remainder of the run.

Comparing Figs. 2 and 4, the time coincidence of the rapid pressure drops and the rapid drop in the observed velocity V' is apparent. Both occurrences are a manifestation that the laminar-turbulent interface is passing the pipe outlet at x/D of 475. Prior to $t\sqrt{gh_0}/L$ of 1.38 the flow is laminar at the outlet. During this time a laminar-turbulent interface is moving toward the outlet. The flow is turbulent upstream from the interface. As explained in the preceding paragraph, the piezometric head is higher in the turbulent flow immediately behind the interface than in the laminar flow immediately preceding the interface. The outlet of the pipe is a station of fixed piezometric head level since the liquid jet is projected into the atmosphere. Thus as the laminar-turbulent interface passes the outlet, the piezometric head line is rapidly lowered just upstream from the outlet. The effect is a pivoting of the piezometric head line. This rapid pivoting of the piezometric head line results in a piezometric head drop at every measuring station. The magnitude of this drop is directly proportional to the distance from the inlet. This effect is clearly illustrated in Fig. 2 at the time $t\sqrt{gh_0}/L$ of 1.38.

With this preliminary knowledge concerning the movement of turbulence, regions can be definitely located in which the flow is laminar. For example, on Fig. 2 between the time $t\sqrt{gh_o}/L$ of 0.715 and 1.06 the flow is laminar between the x/D stations 379 and 475, and prior to $t\sqrt{gh_o}/L$ of 0.715 the flow is laminar between the x/D stations of 284 and 475.

The piezometric head lines are indicative that the laminar flow regions are one-dimensional. At constant values of time $t\sqrt{gh_o}/L$ the measured values of piezometric head were plotted as a function of x/D. In addition to the data obtained from the pressure transducers, the constant zero piezometric head at the outlet was utilized. Since the piezometric head lines were straight at a given time in this laminar flow region, the conclusion was that the region was also a one-dimensional flow region as visualized in the derivation of Eq. (2). A contributing factor in the existence of this one-dimensional downstream laminar flow region is the presence of upstream turbulent flow regions, since an upstream turbulent flow region has the effect of isolating the inlet. Thus the downstream laminar flow region is similar to flow in an infinitely long pipe since the boundary-layer thickness, piezometric head gradient, and developing velocity profile are functions only of time.

The slopes of these piezometric head lines were determined and plotted. These slope values are shown as points on Fig. 5 for the run being discussed. In order to incorporate this experimental data into Eq. (2), an analytic function for $g(\gamma)$ must be selected that approximates the empirical results. A very simple function was selected, that is, $\partial p^*/\partial x$ is proportional to $\cos(\pi t/2t^*)$ in which $t^*\sqrt{gh_o}/L$ is

empirically defined as shown on Fig. 5. The value of $t^* \sqrt{gh_o}/L$ is dependent upon the experimental parameters as well as the time and position of turbulence inception. The function for $g(\Upsilon)$ was introduced into Eq. (2) and the integration performed. The resulting expression for the time-developing velocity profile is

$$\frac{v}{V} = \frac{\displaystyle\sum_{n=1}^{\infty} \frac{J_o (a_n \beta)}{a_n^3 J_1 (a_n)} \left[\frac{\left(\cos \frac{\pi}{2} \frac{t}{t^*} + \frac{\pi}{2 a_n^2 \alpha^*} \sin \frac{\pi}{2} \frac{t}{t^*} \right) - e^{-a_n^2 \alpha^* (t/t^*)}}{1 + \left(\frac{\pi}{2 a_n^2 \alpha^*} \right)^2} \right]}{2 \displaystyle\sum_{n=1}^{\infty} \frac{1}{a_n^4} \left[\frac{\left(\cos \frac{\pi}{2} \frac{t}{t^*} + \frac{\pi}{2 a_n^2 \alpha^*} \sin \frac{\pi}{2} \frac{t}{t^*} \right) - e^{-a_n^2 \alpha^* (t/t^*)}}{1 + \left(\frac{\pi}{2 a_n^2 \alpha^*} \right)^2} \right]} \quad (3)$$

All terms of Eq. (3) have been previously defined except α^* which is $\upsilon t^*/r_o^2$.

Values of v/V were computed in systematic steps so that by interpolation of the computed results, these results could be applied to all experimental runs. The first nine zero-roots of the Bessel function were used in the numerical computations. The range of the other variables were as follows: $0 < \beta < 1$, $0.01 < \alpha^* < 0.05$, and $0.2 < t/t^* < 1.0$. Values of the linear momentum correction coefficient C_m were then computed using numerical graphical methods. Hence to determine the temporal variation of C_m for any experiments run only the value of $t^* \sqrt{gh_o}/L$ was required.

The analytical solution does not cover the complete temporal range of laminar flow. An empirical method was utilized in order to extrapolate the analytical solution. The method used is based upon observed velocity data. At the time of transition from laminar flow to turbulent flow at the pipe outlet, there is a sharp discontinuity in observed velocity, as shown in Fig. 4. However there can be no discontinuity in the true mean velocity. Thus the observed discontinuity must be due to the difference in C_m of the laminar flow and turbulent flow. Hence at the time of transition

$$(C_m)_{\text{laminar}} = 1.02 \; \frac{(V'/\sqrt{2gh_o})_{\text{laminar}}}{(V'/\sqrt{2gh_o})_{\text{turbulent}}}$$

since $(C_m)_{\text{turbulent}}$ is equal to 1.02. The value of C_m of 1.02 for turbulent flow is based upon the seventh-root law of velocity distribution.

The temporal variation of C_m and the corresponding corrected velocity-time curves for Runs 20-29 are shown in Figs. 6-15.

BOUNDARY SHEAR INVESTIGATION

The experimental data, corrected and interpreted as described in the preceding paragraphs, presents an avenue of investigation into the little-known realm of unsteady shear forces.

One-dimensional equation of motion.—The complete one-dimensional differential equation of motion is necessary to determine boundary shear forces from experimentally determined values of pressure and velocity. The fluid element utilized in the derivation is, as shown in Fig. 16, a cross

sectional element of the fluid in the pipe which is dx in length. The external forces on the fluid element in the x direction are the resultant pressure force on the end areas and the boundary shear force. The momentum equation for this element is

$$- \frac{\partial p}{\partial x} \, dx \, \frac{D^2 \pi}{4} - \tau_o \, D \pi dx = \frac{\partial}{\partial x} \left[\int^A \rho \, v dQ \right] dx + \frac{\partial}{\partial t} \left[\int^{\Psi} \rho \, v d\Psi \right] \quad (4)$$

The first term on the right side of Eq. (4) is the difference of momentum flux through the end areas of the fluid element. Utilizing the one-dimensional method,

$$\int^A \rho \, v dQ = C_m \, \rho \, QV = C_m \, \rho \, V^2 \, \frac{D^2 \pi}{4} \quad (5)$$

The second term on the right side of Eq. (4) is the time rate of change of linear momentum of the particles on the interior of the element. The symbol Ψ is used to represent volume.

$$d\Psi = dA \, dx$$

The end areas of the element are chosen so that dx is a constant for every dA. Thus

$$\frac{\partial}{\partial t} \int^{\Psi} \rho \, v d\Psi = \frac{\partial}{\partial t} \left[\int^A \rho \, v dA \right] dx = \rho \, \frac{\partial Q}{\partial t} \, dx \quad (6)$$

Since,

$$Q = VA$$

and since Q is a function of time alone

$$\frac{\partial Q}{\partial t} = \frac{D^2 \pi}{4} \frac{dV}{dt} \tag{7}$$

Introducing Eqs. (5), (6), and (7) into Eq. (4) and dividing by the elemental volume, the desired differential equation is

$$-\frac{\partial p}{\partial x} - \frac{4\tau_o}{D} = \rho V^2 \frac{\partial C_m}{\partial x} + \rho \frac{dV}{dt} \tag{8}$$

Eq. (8) may be further reduced. There is no axial variation (a short distance downstream from the inlet) of the velocity distribution in turbulent flow; also the corrected experimental data in laminar flow excludes any axial variation. Thus, in these cases $\frac{\partial C_m}{\partial x} = 0$, and

$$-\frac{\partial p}{\partial x} - \frac{4\tau_o}{D} = \rho \frac{dV}{dt} \tag{9}$$

Several parameters may be used to describe the boundary shear. The Darcy-Weisbach resistance coefficient, f, is commonly used in conduit flow. Since the steady flow relationships of f are well established and in common use, this parameter is used throughout the following analysis. In turbulent flow f is an adequate parameter since the shear varies with V^2. In laminar flow a better parameter might be desired due to different shear processes, because in laminar flow the shear varies with V. However no attempt was made to revert from the conventional f. Since, by definition

$$\tau_o = f \rho \frac{V^2}{8} \tag{10}$$

then

$$- \frac{\partial p}{\partial x} - \frac{f \, \rho V^2}{2D} = \rho \frac{dV}{dt} \tag{11}$$

Converting to dimensionless form

$$f = \frac{- \dfrac{\partial (h/h_o)}{\partial (x/D)} - \dfrac{\sqrt{2}\,D}{L} \dfrac{d(V/\sqrt{2gh_o})}{d(t\sqrt{gh_o}/L)}}{\left(\dfrac{V}{\sqrt{2gh_o}}\right)^2} \tag{12}$$

Method of investigation.--The boundary shear, as reflected in the value

of f, may be determined at any time by utilizing the experimental data

in the form as described in the preceding section, and the one-dimen-

sional equation of motion, Eq. (12). For purposes of illustrating the

method of investigation the data of Run 29 are utilized.

Fig. 17 represents in dimensionless form the temporal variation

of the piezometric head gradient. Both the turbulent and laminar gradients

are shown on the one plot. On Fig. 17 it can be seen that both types of

flow may exist in the pipe simultaneously.

Fig. 6 depicts the variation of the corrected dimensionless mean

velocity. The dimensionless acceleration as shown in Fig. 18 was ob-

tained by graphical means from Fig. 6.

Values of the above three variables may be read from the corres-

ponding plots at simultaneous times and f computed by Eq. (12). The value

of $- \dfrac{\partial (h/h_o)}{\partial (x/D)}$ used depends upon whether laminar or turbulent shear is

being investigated.

Tabulated results for Runs 20-29 appear in the Appendix.

Interpretation of results.—Dimensionless boundary shear, f, in smooth pipes with steady flow is a function of only the Reynolds number. The existence of other independent variables is likely with unsteady flow. Parameters of unsteadiness may have a direct or indirect influence upon f.

The shear processes differ in laminar and turbulent flow.

Boundary shear in laminar flow depends solely upon the velocity distribution and fluid viscosity as represented by

$$\tau_o = - \mu \left. \frac{dv}{dr} \right|_{r = r_o} \tag{13}$$

Hence any effects of unsteadiness must be embodied in the instantaneous velocity profile. Eq. (13) may be expressed in terms of f,

$$f = \frac{1}{R} \left[- \frac{8D}{V} \frac{dv}{dr} \right] \Bigg|_{r = r_o} \tag{14}$$

Thus in laminar flow

$$f = \phi \, (\, R, \text{ velocity profile characteristics}) \tag{15}$$

The Reynolds number R may be eliminated from consideration by using a ratio of unsteady shear f and steady shear f_s, that is, f_s/f. Thus all laminar unsteady shear values are compared with the Hagen-Poiseuille equation for fully developed laminar flow,

$$f = \frac{64}{R} \tag{16}$$

Elimination of R reduces the shear analysis to

$$\frac{f_s}{f} = \phi \text{ (velocity profile characteristics)} \tag{17}$$

The velocity profile characteristics are difficult to express in parameter form, since the developing velocity distribution at any time is dependent upon initial conditions and the intervening flow conditions, that is, history of the flow. If one may assume that at any stage of development the velocity profiles are related regardless of the flow history, then a single parameter such as the dimensionless displacement boundary-layer thickness, δ^*/r_o, may be utilized to describe velocity profile characteristics. The displacement boundary layer thickness in pipe flow is defined in the expression

$$Q = \int_0^{r_o} v \, 2 \pi r \, dr = v_c \, (r_o - \delta^*)^2 \pi \tag{18}$$

where v_c is the core or centerline velocity. Thus based upon the above assumption,

$$\frac{f_s}{f} = \phi \, (\delta^*/r_o) \tag{19}$$

Laminar shear data are shown in Fig. 19 in this form.

An analysis of shear from the solution presented in Eq. (3) was utilized for comparison with experimental data, Fig. 19, and to evaluate the soundness of the preceding assumption. By differentiation of Eq. (3) and by subsequent algebraic operation the following expression is obtained

$$\frac{f_s}{f} = \frac{\displaystyle\sum_{n=1}^{\infty} \frac{1}{a_n^4} \left[\frac{\left(\cos\frac{\pi}{2}\frac{t}{t^*} + \frac{\pi}{2a_n^2\alpha^*} \sin\frac{\pi}{2}\frac{t}{t^*} \right) - e^{-a_n^2\alpha^* t/t^*}}{1 + \left(\frac{\pi}{2a_n^2\alpha^*} \right)^2} \right]}{\displaystyle\sum_{n=1}^{\infty} \frac{1}{a_n^2} \left[\frac{\left(\cos\frac{\pi}{2}\frac{t}{t^*} + \frac{\pi}{2a_n^2\alpha^*} \sin\frac{\pi}{2}\frac{t}{t^*} \right) - e^{-a_n^2\alpha^* t/t^*}}{1 + \left(\frac{\pi}{2a_n^2\alpha^*} \right)^2} \right]} \tag{20}$$

for shear resulting from the approximated cosine variation of the piezo-metric head gradient. Values of $\frac{f_s}{f}$ and $\frac{\delta^*}{r_o}$ were computed for α^* of 0.01, 0.02, 0.03, 0.04, and 0.05. This range of α^* encompassed the entire experimental range. In addition, shear values were computed with $\alpha^* \to \infty$, which represents the outer limit of the cosine solution. A cosine variation with an infinite period represents the case of flow establishment with a constant piezometric head gradient. The results of these computations are presented on Fig. 20.

The analytical results shown on Fig. 20 are conclusively indicative that a single parameter representation of the velocity profile characteristics is inadequate for singular correlation of laminar shear for all flow conditions. The analytical shear results are dependent upon a second parameter, α^*, which is a parameter of temporal flow development in Eq. (3). Thus one may conclude that there is not an unique

velocity profile relation for unsteady laminar flow; rather the velocity profile shape or the shear at any stage of flow development is dependent upon temporal flow history.

A comparison of the analytical results with the experimental shear data indicates that the experimental and analytical shear values are in close agreement. However due to experimental scatter the minor effect of the various flow histories is not apparent.

Shear processes in turbulent flow are complicated by the complex pattern of motion which varies continuously with time. Nevertheless, previous investigation has shown that for steady turbulent flow in smooth circular pipes

$$\tau_o = \phi (V, D, \rho, \mu)$$ (21)

or in dimensionless form

$$f = \frac{\tau_o}{\rho V^2/8} = \phi (R)$$ (22)

One may assume that unsteadiness introduces another independent variable, the accelerative state of the fluid, dV/dt, or

$$\tau_o = \phi (V, D, \rho, \mu, \frac{dV}{dt})$$ (23)

The assumption, that the effect of unsteadiness is instantaneous, rather than historical as in laminar flow, is based upon the inherent diffusing action of turbulence. The continuous turbulent diffusion of the fluid eliminates any physical concept of a historical effect; hence the effect of unsteadiness must be independent of initial and intervening flow

conditions. Thus based upon this assumption,

$$f = \tau_o / \varrho V^2/8 = \phi (\mathbb{R}, \frac{D}{V^2} \frac{dV}{dt}) \tag{24}$$

The Blasius equation for steady turbulent flow

$$f \cong \frac{0.3164}{\mathbb{R}^{\frac{1}{4}}} \tag{25}$$

was used as a reference for the experimentally determined values of f. This was done by utilizing the ratio of the experimental value of f with the corresponding steady flow value, f_s, a procedure which is possible only if the assumption is made that any accelerative effects are manifested only in the constant, that is, the general equation is expressed by

$$f = \frac{C}{\mathbb{R}^{\frac{1}{4}}} \tag{26}$$

and

$$C \cong \phi \left[\frac{D}{V^2} \frac{dV}{dt} \right] \tag{27}$$

Based upon the above assumption, at the point of maximum velocity or zero acceleration the ratio of f to f_s must equal unity. The experimental results did not exhibit this property, but had an erratic variation of within ± 5%. This variation is attributed to experimental error and approximations used in correcting the mean velocity. To aid in the presentation of results the experimental values were corrected by referencing, for each run, all values of f to the steady flow value, that is,

$$\frac{f}{f_s} \bigg|_{\frac{D}{V^2} \frac{dV}{dt} = 0} = 1 \tag{28}$$

The results shown in Fig. 21 show a definite variation of f with a variation in the acceleration parameter $\frac{D}{V^2} \frac{dV}{dt}$. Although the scatter of the data and limited range of values prevent quantitative conclusions, the consistent variation of f indicates the qualitative effect of unsteadiness.

CONCLUSIONS

The following conclusions may be drawn from this unsteady shear investigation:

(1) The one-dimensional solution of the Navier-Stokes equations is an excellent investigative approach for determining the flow characteristics of unsteady laminar flow in a pipe. The determination of the mean velocity as a function of time involved the incorporation of the experimentally determined laminar piezometric head gradient into the Navier-Stokes equations. The laminar velocity distribution characteristics as a function of time were then determined from the solution of the Navier-Stokes equations. With the laminar velocity distribution characteristics determined in this manner, the mean velocity of the flow could be determined from the photographic record of the jet. The one-dimensional equation of pipe flow was then utilized in order to determine the boundary shear stress. This entire procedure was entirely satisfactory.

(2) The experimental method could be simplified during the time that a laminar flow region existed in the pipe. The mean

velocity of the flow as a function of time could be determined from the solution of the Navier-Stokes equations in which the experimentally determined laminar piezometric head gradient was utilized. In this manner, the need of jet photography would be eliminated. However this simplified scheme is dependent upon the presence of a laminar flow region during the time of interest; whereas, the method utilizing jet photography is applicable even though the flow were turbulent throughout the pipe.

(3) A single parameter representation of velocity profile characteristics is inadequate for singular correlation of laminar shear for all flow conditions. Thus there is no unique velocity profile relation for unsteady laminar flow. Laminar shear at any stage of flow development is dependent upon initial conditions and intervening flow conditions.

(4) The experimental turbulent shear data are indicative of a qualitative effect of unsteadiness on turbulent shear. An increase in f is observed with fluid deceleration and a corresponding decrease is observed with fluid acceleration.

FIGURES
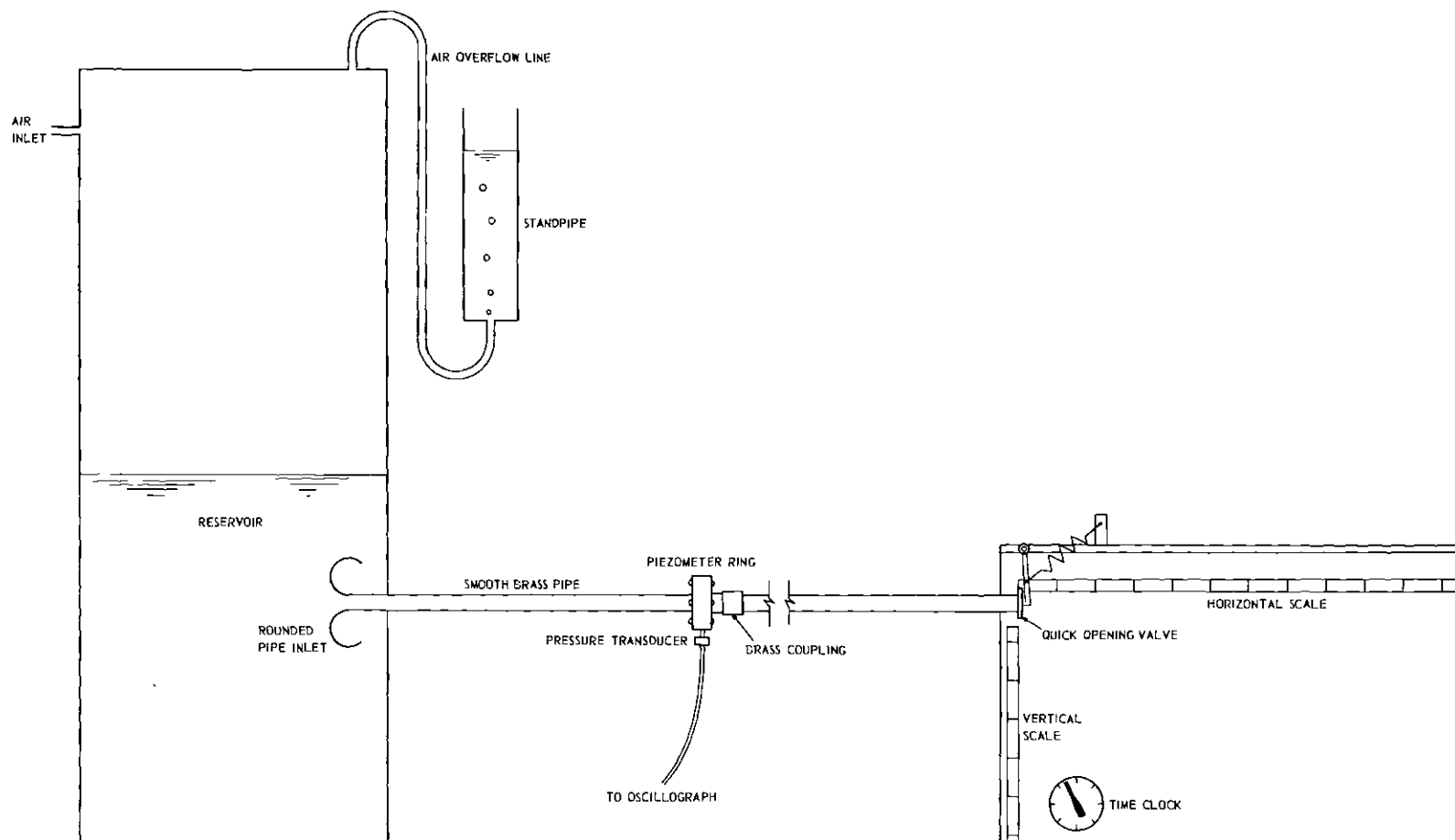
Figure 1.　Schematic Drawing of Equipment.
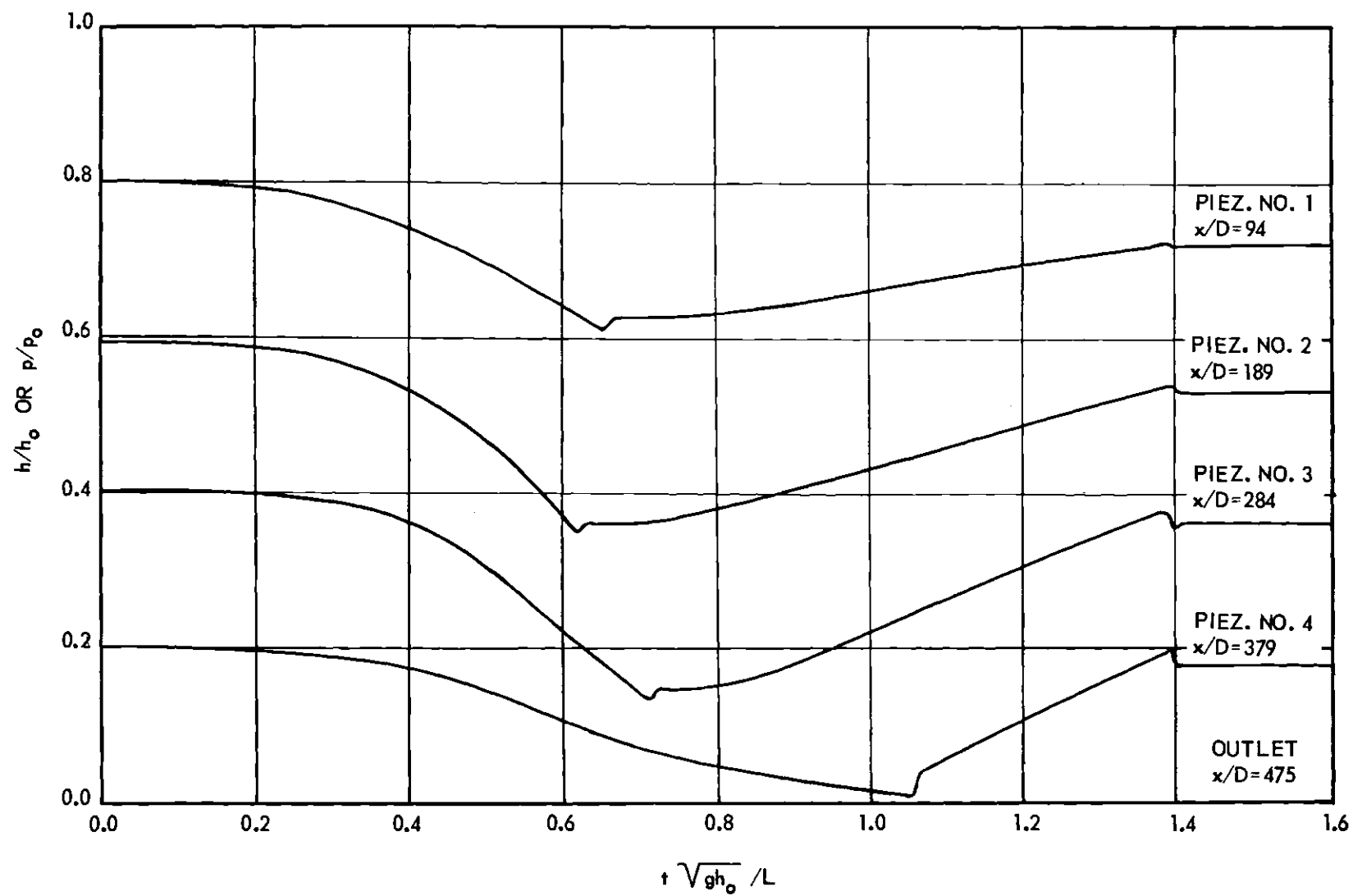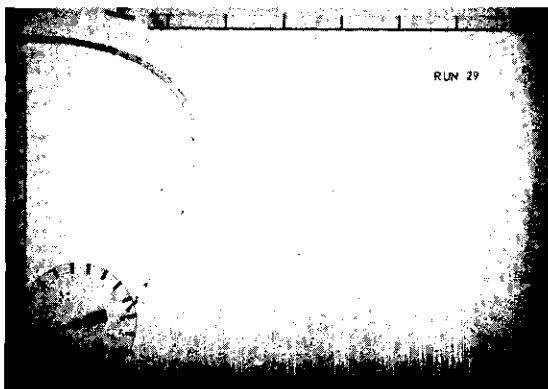
Figure 2. Pressure-time Curves of Runs 29 and 29a.
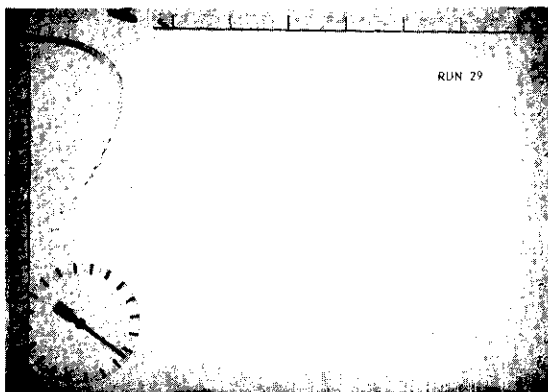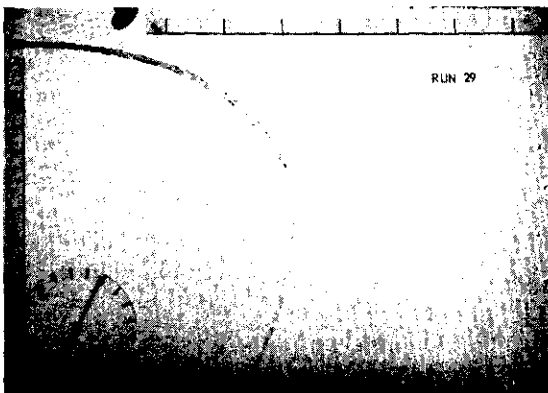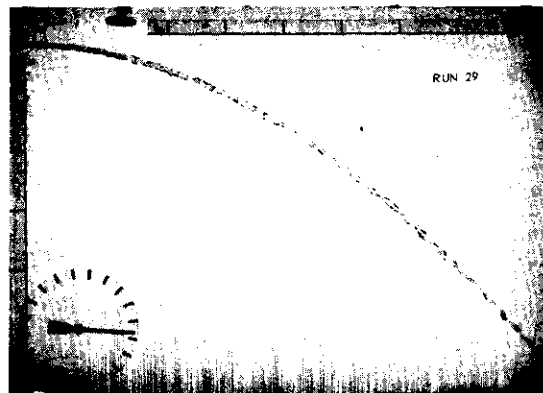
(a) T = 0.355 SEC.
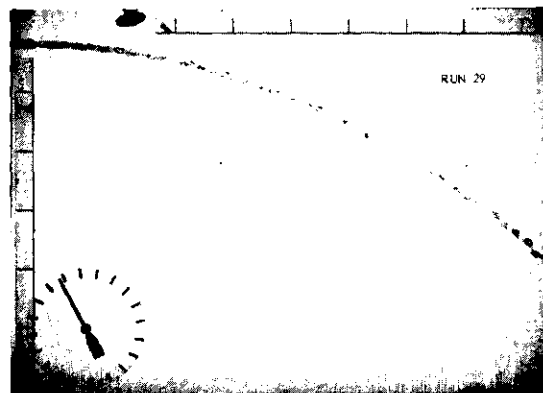
(b) T = 0.466 SEC.

(c) T = 0.511 SEC.

(d) T = 1.222 SEC.
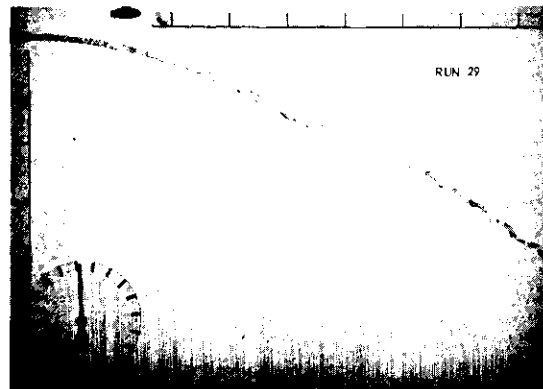
(e) T = 1.607 SEC.

(f) T = 1.953 SEC.

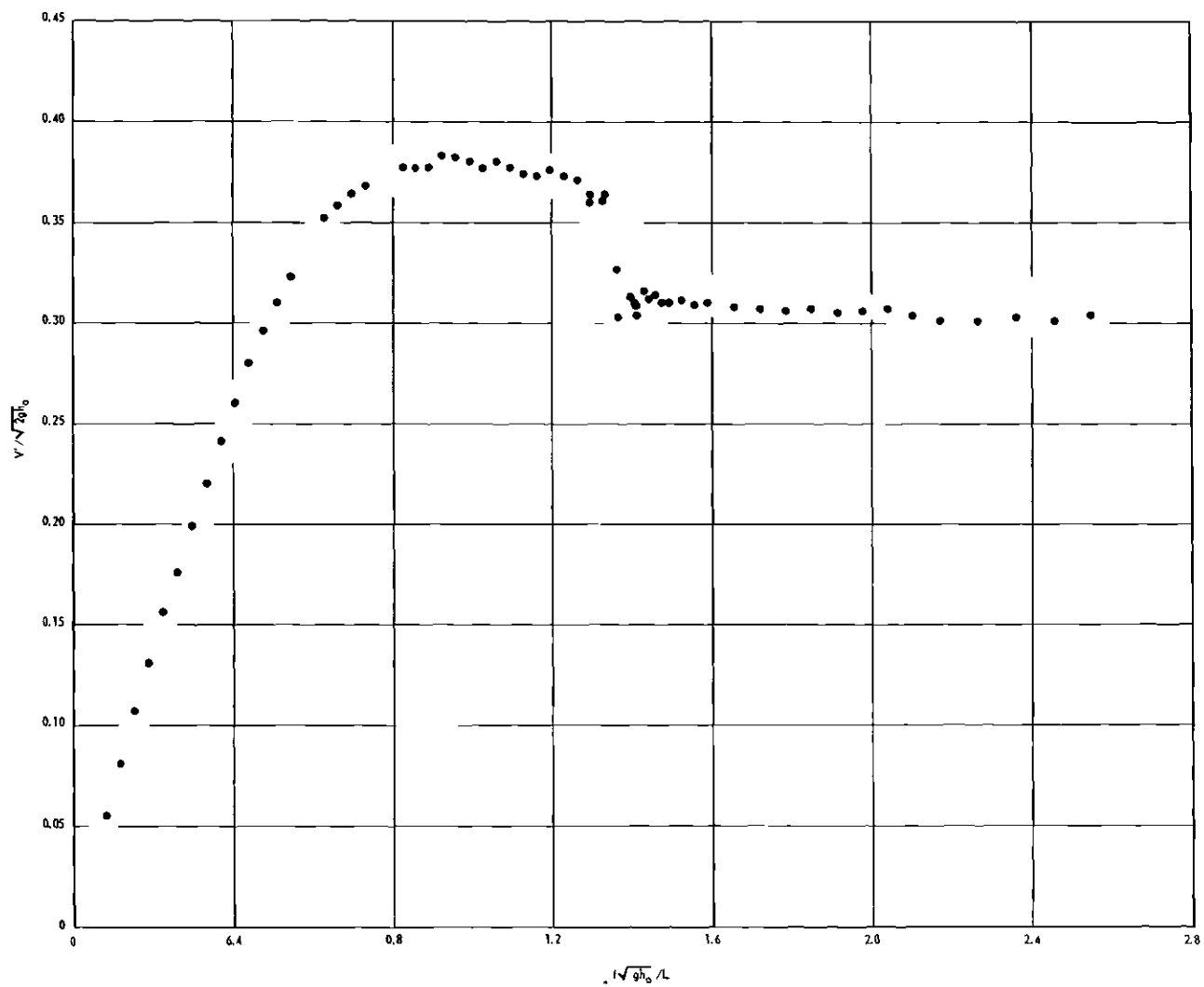Figure 3. Selected Film Strip Data of Run 29.
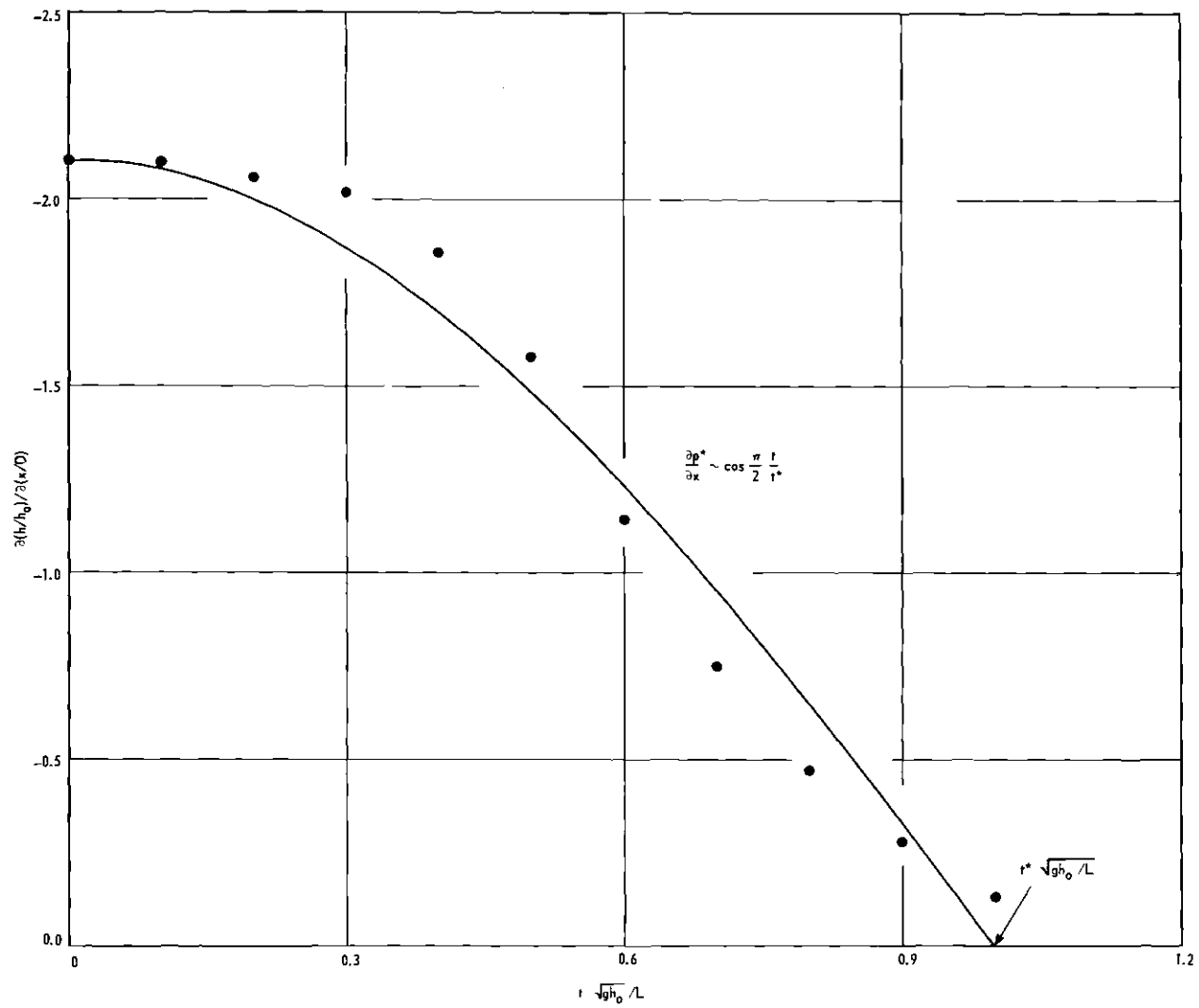
Figure 4.   Observed Velocity-time Data of Run 29.

Figure 5.   Temporal Variation of the Piezometric Head Line Slope of the One-dimensional Laminar Flow of Run 29.
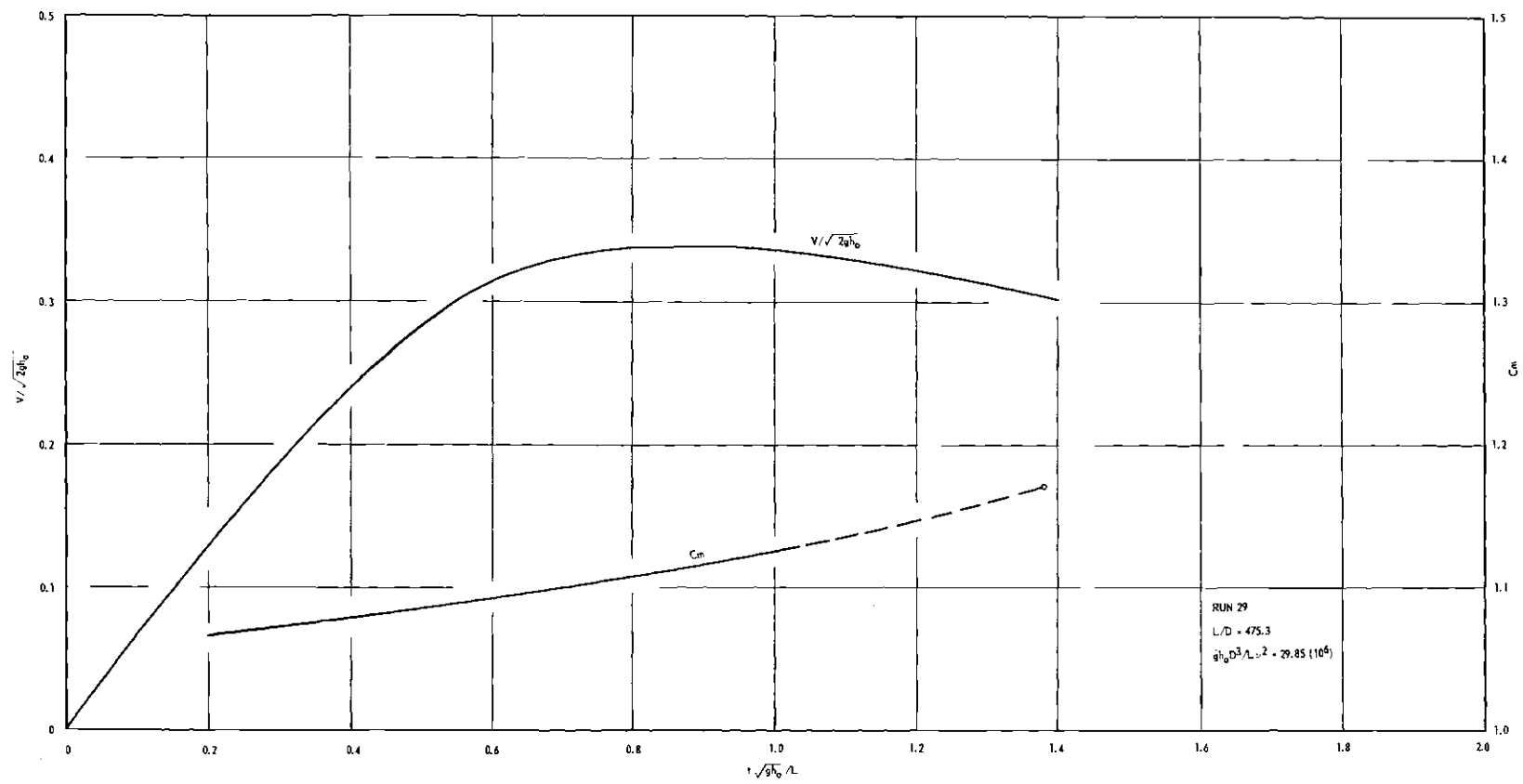
Figure 6. Temporal Variation of Mean Velocity and Linear Momentum Coefficient of Run 29.
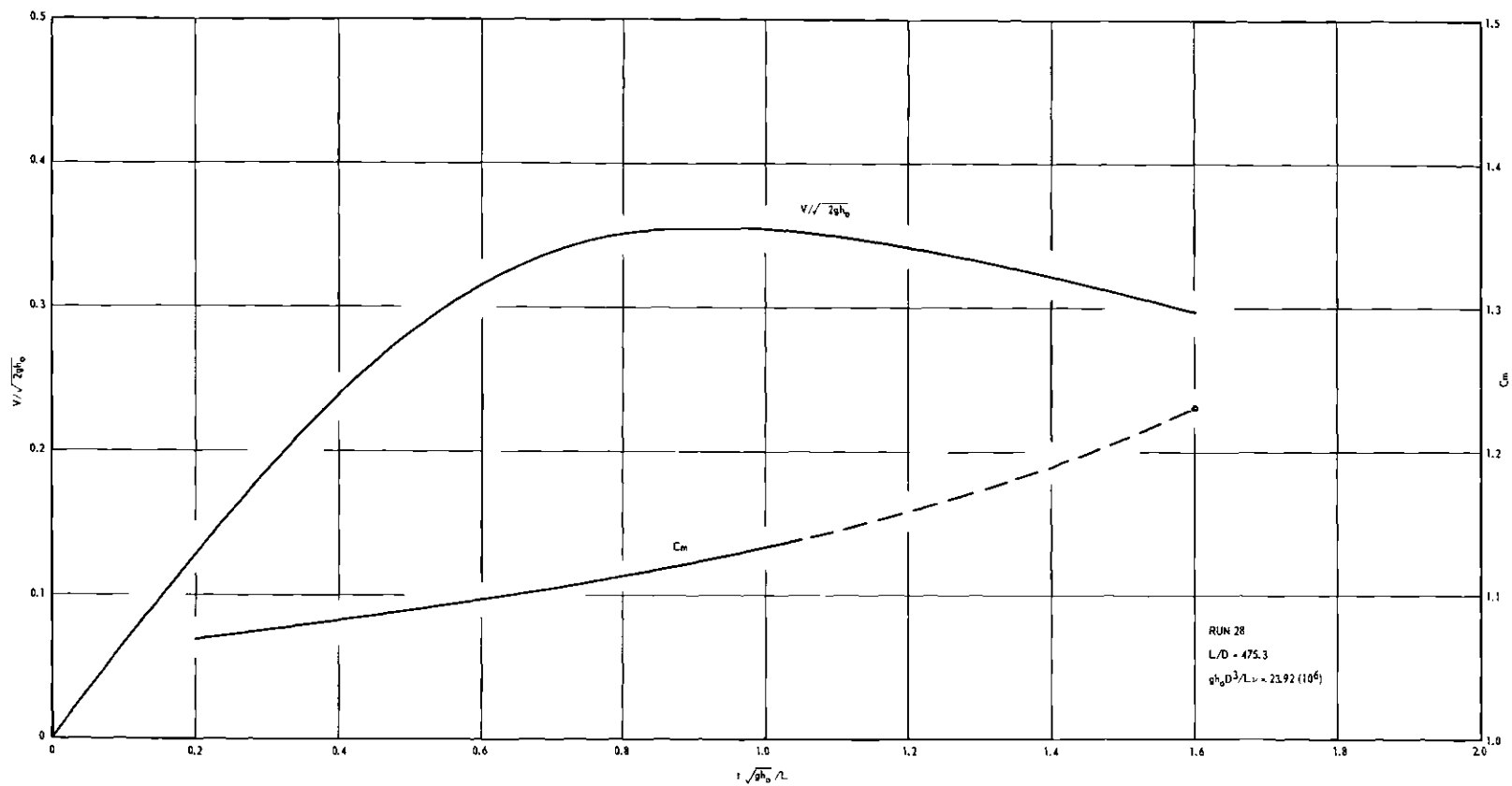
32

Figure 7. Temporal Variation of Mean Velocity and Linear Momentum Coefficient of Run 28.
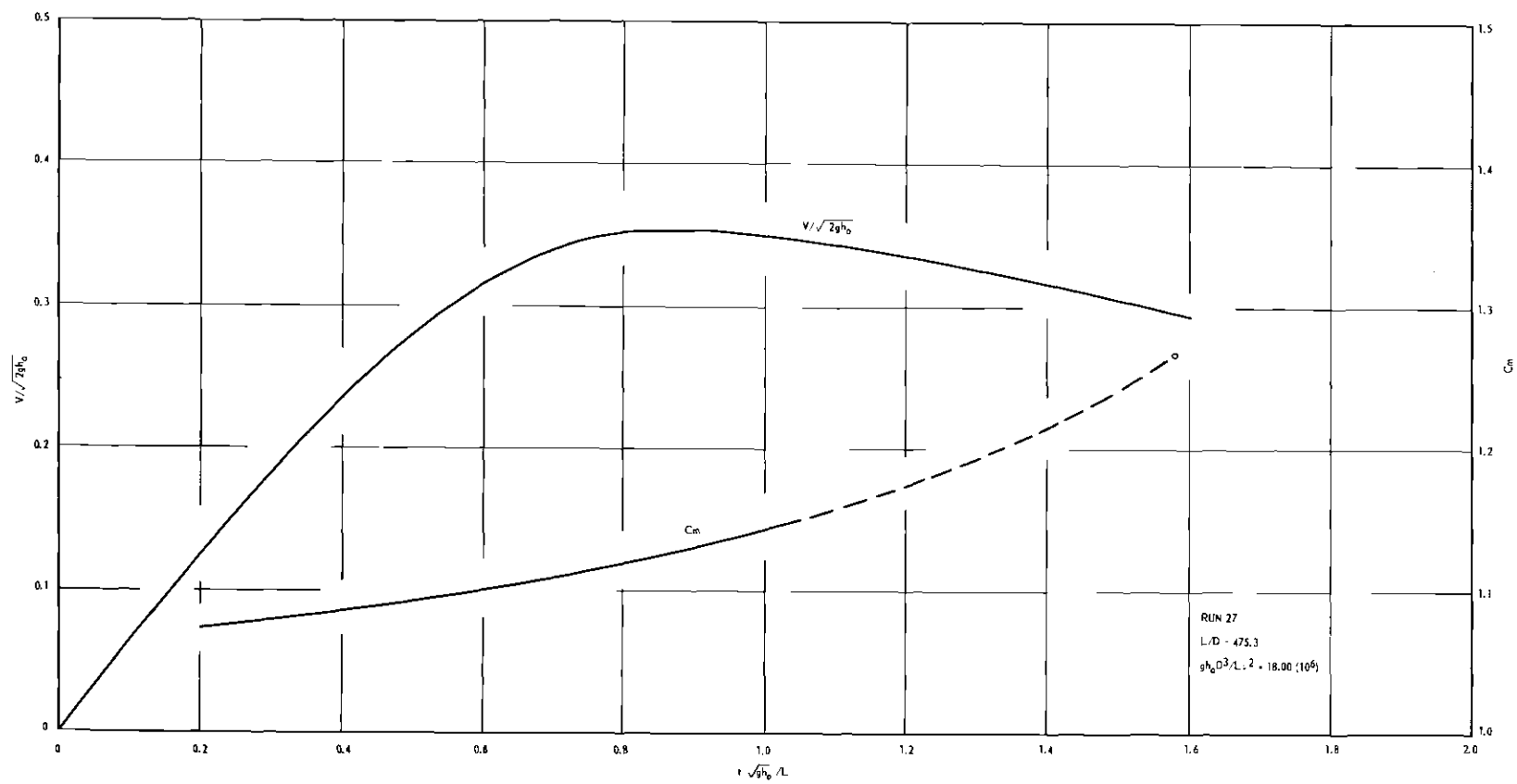
Figure 8. Temporal Variation of Mean Velocity and Linear Momentum Coefficient of Run 27.
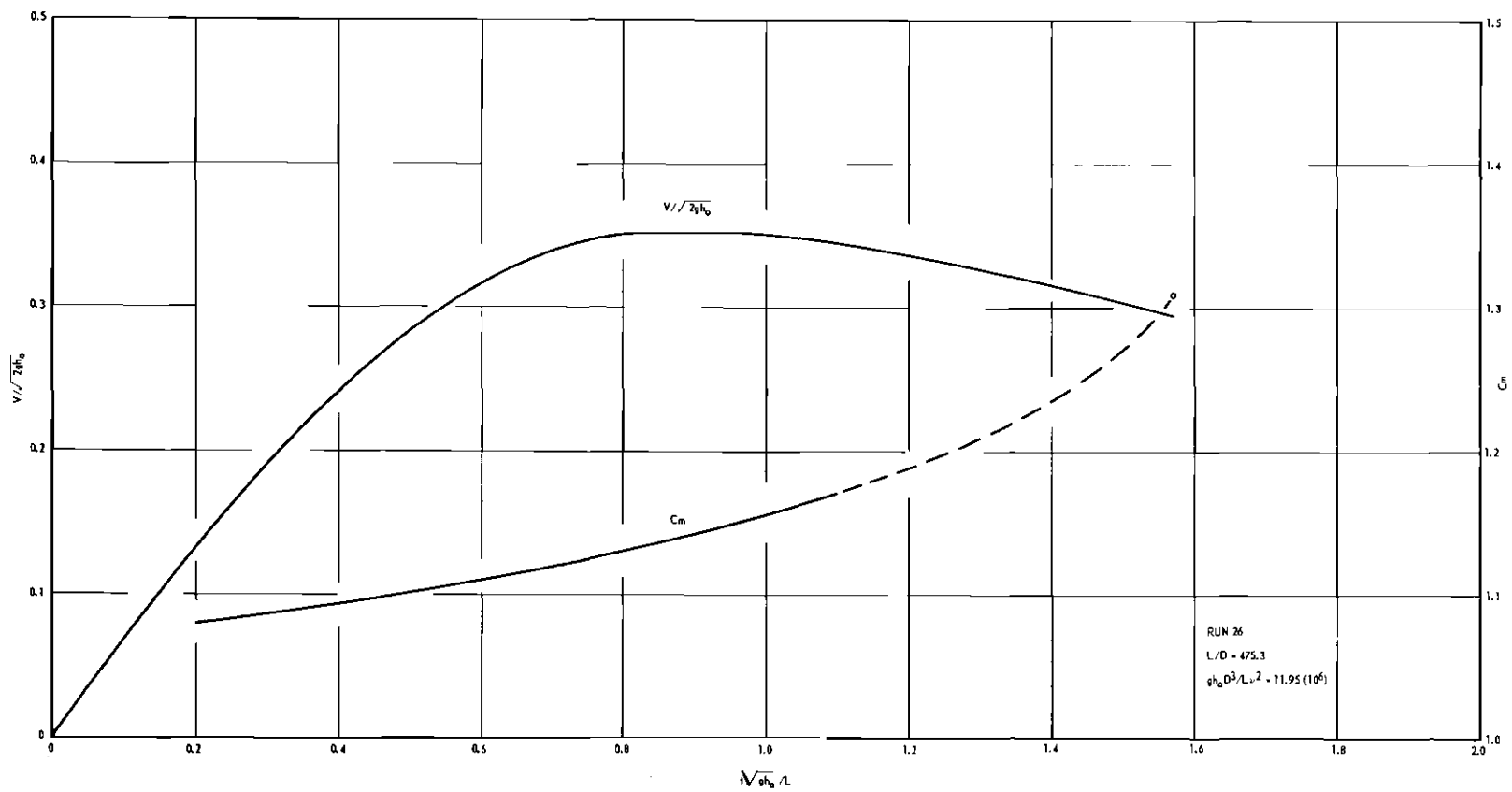
Figure 9. Temporal Variation of Mean Velocity and Linear Momentum Coefficient
of Run 26.

Figure 10. Temporal Variation of Mean Velocity and Linear Momentum Coefficient
of Run 25.

Figure 11. Temporal Variation of Mean Velocity and Linear Momentum Coefficient of Run 24.
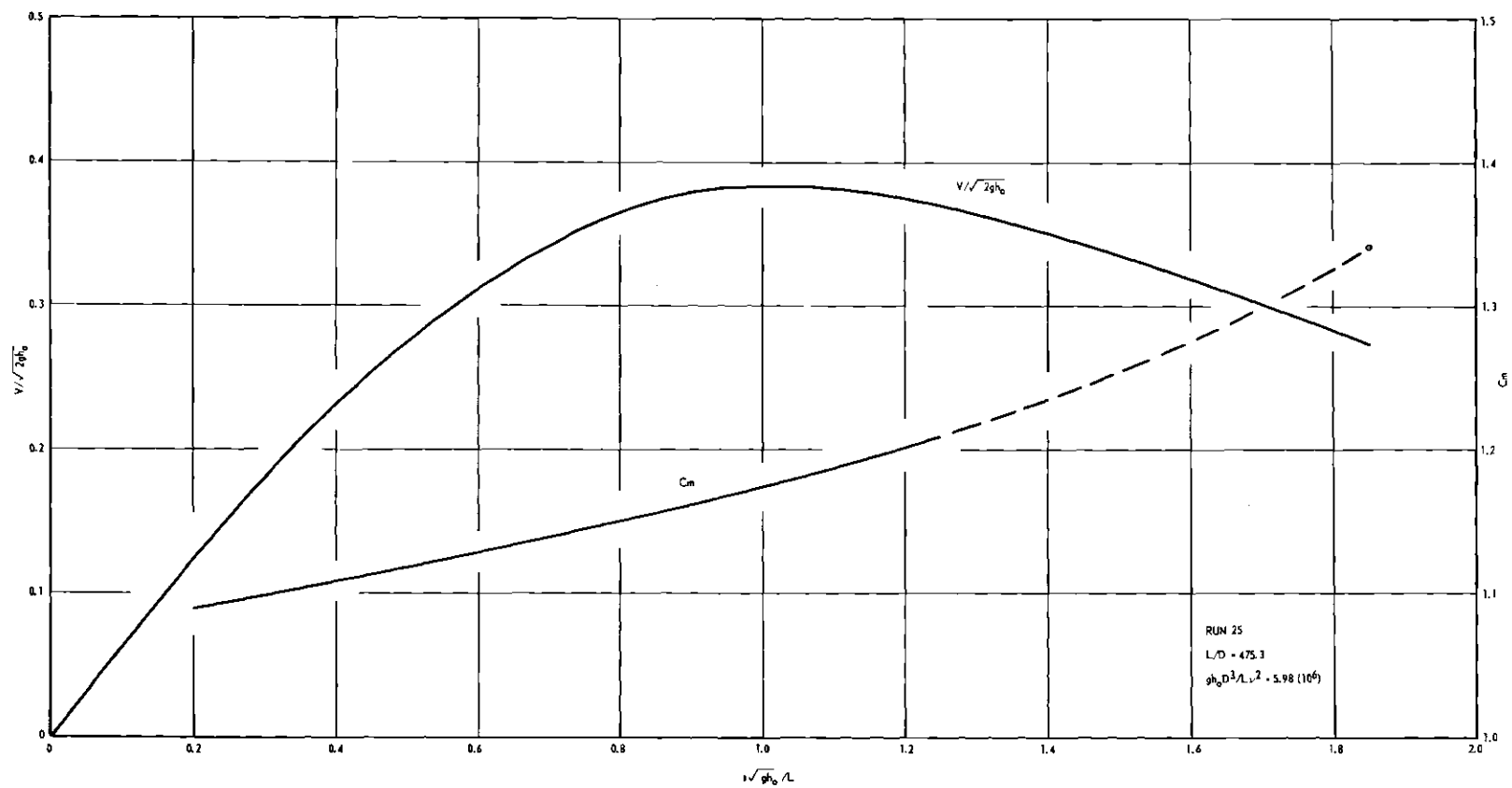
Figure 12. Temporal Variation of Mean Velocity and Linear Momentum Coefficient of Run 23.
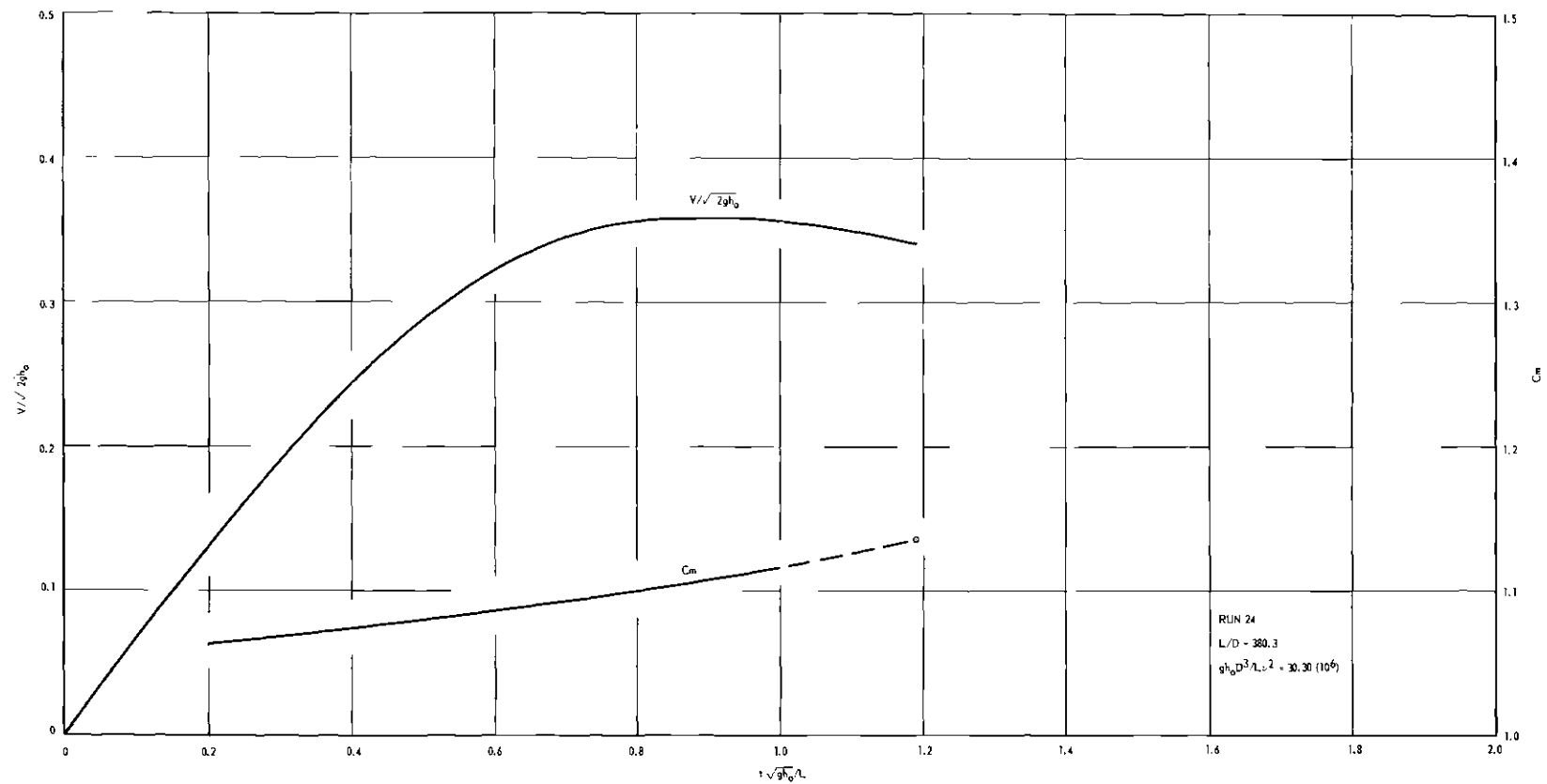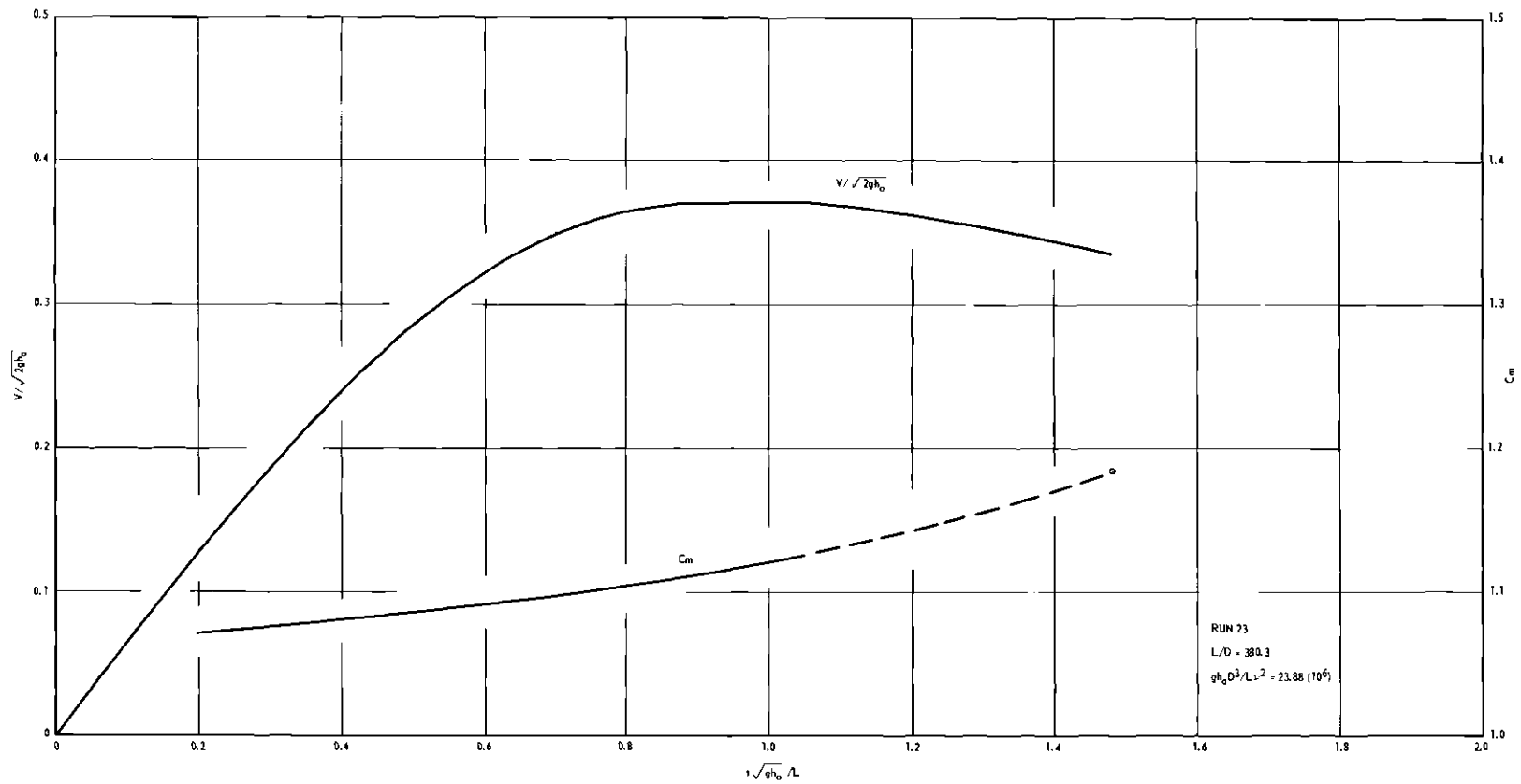
Figure 13. Temporal Variation of Mean Velocity and Linear Momentum Coefficient of Run 22.
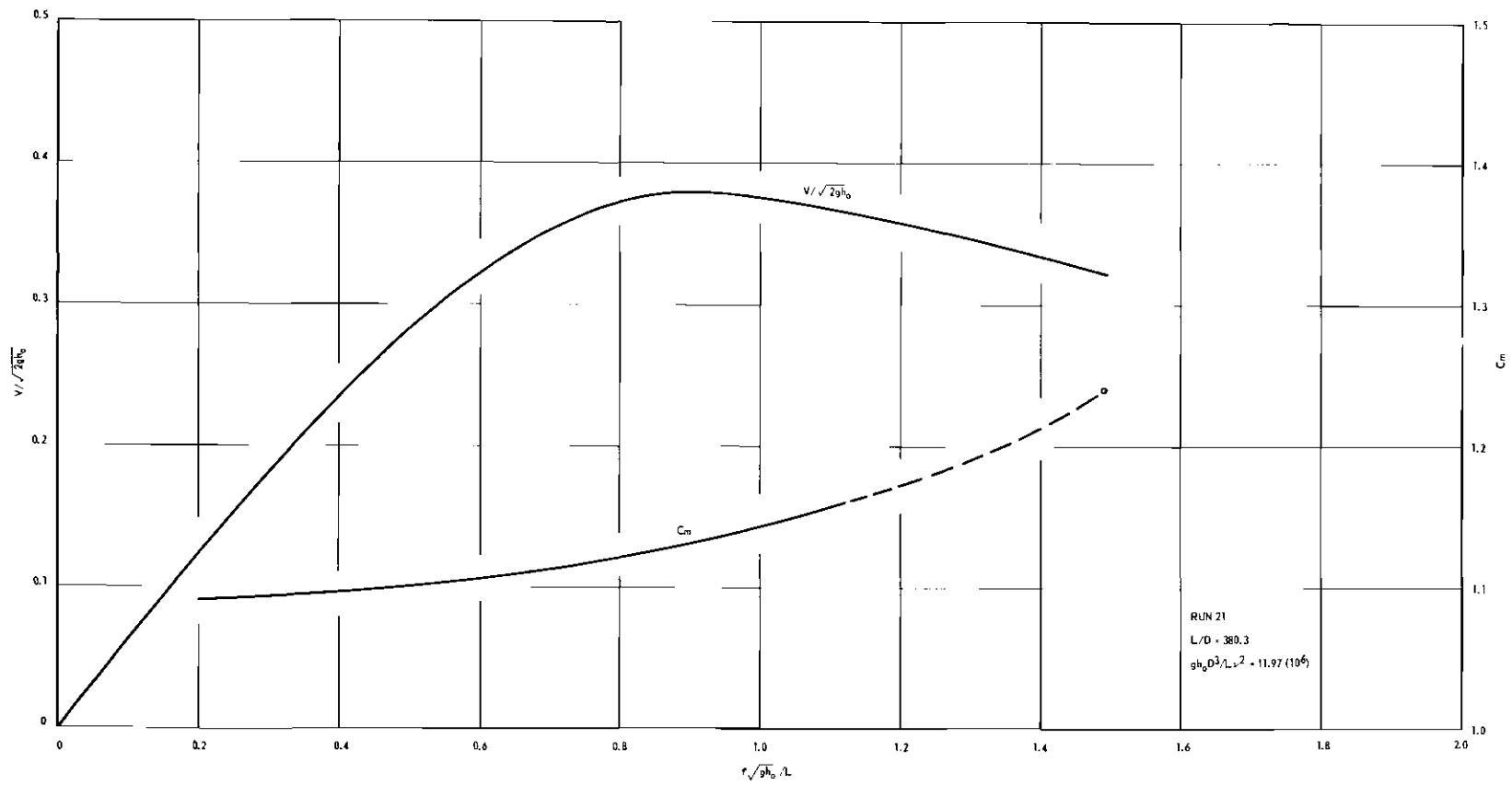
Figure 14. Temporal Variation of Mean Velocity and Linear Momentum Coefficient of Run 21.
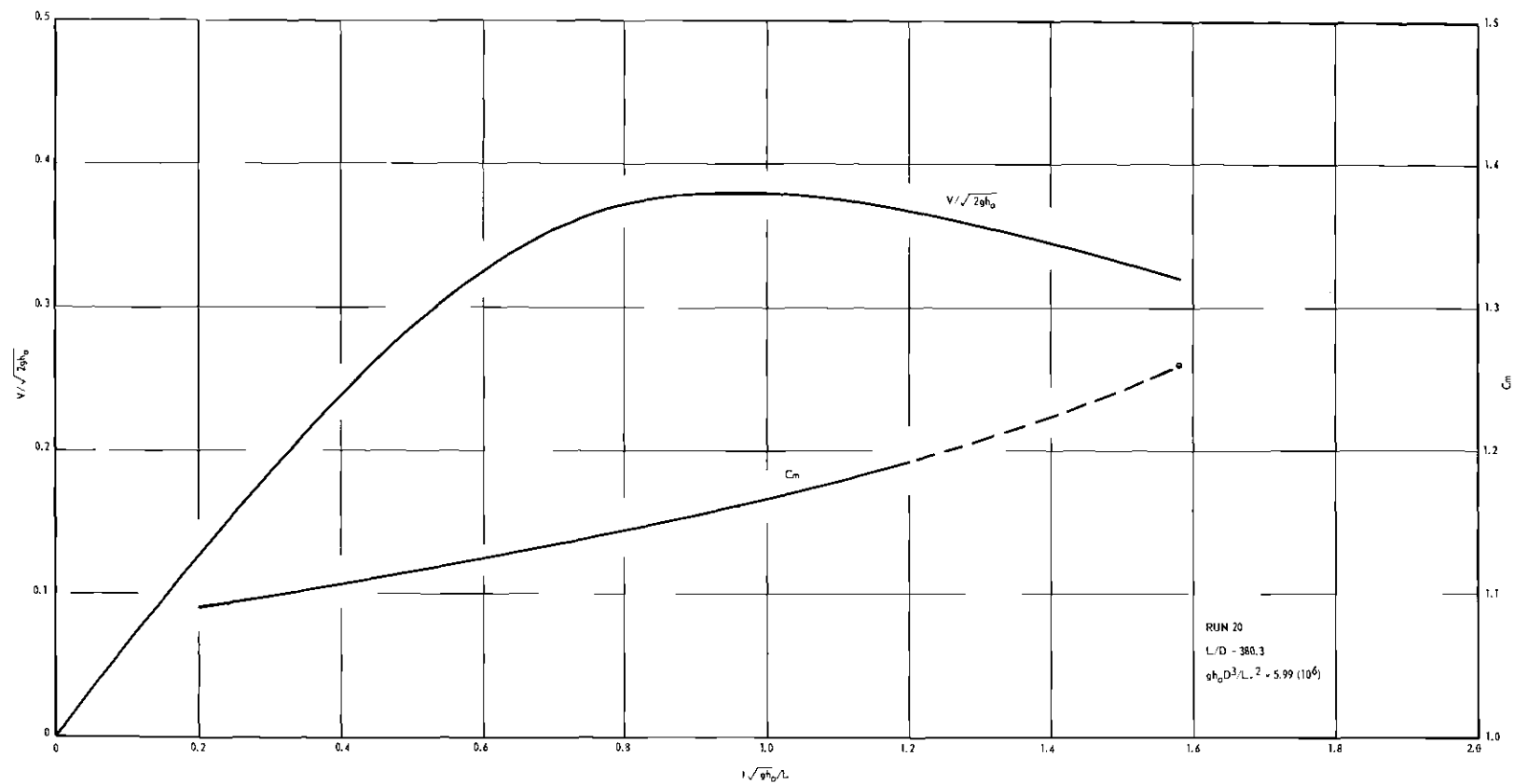
Figure 15.   Temporal Variation of Mean Velocity and Linear Momentum Coefficient
of Run 20.
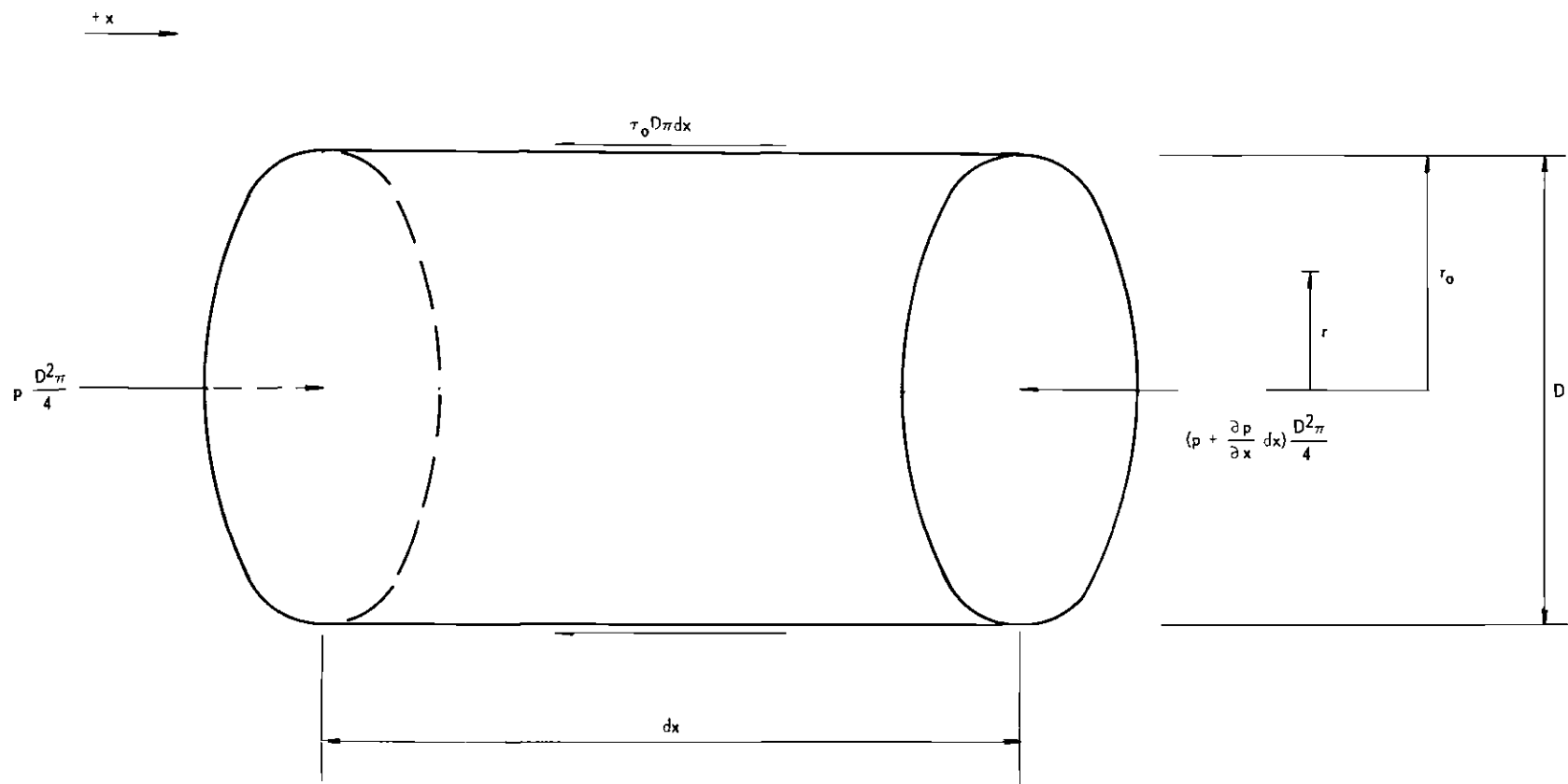
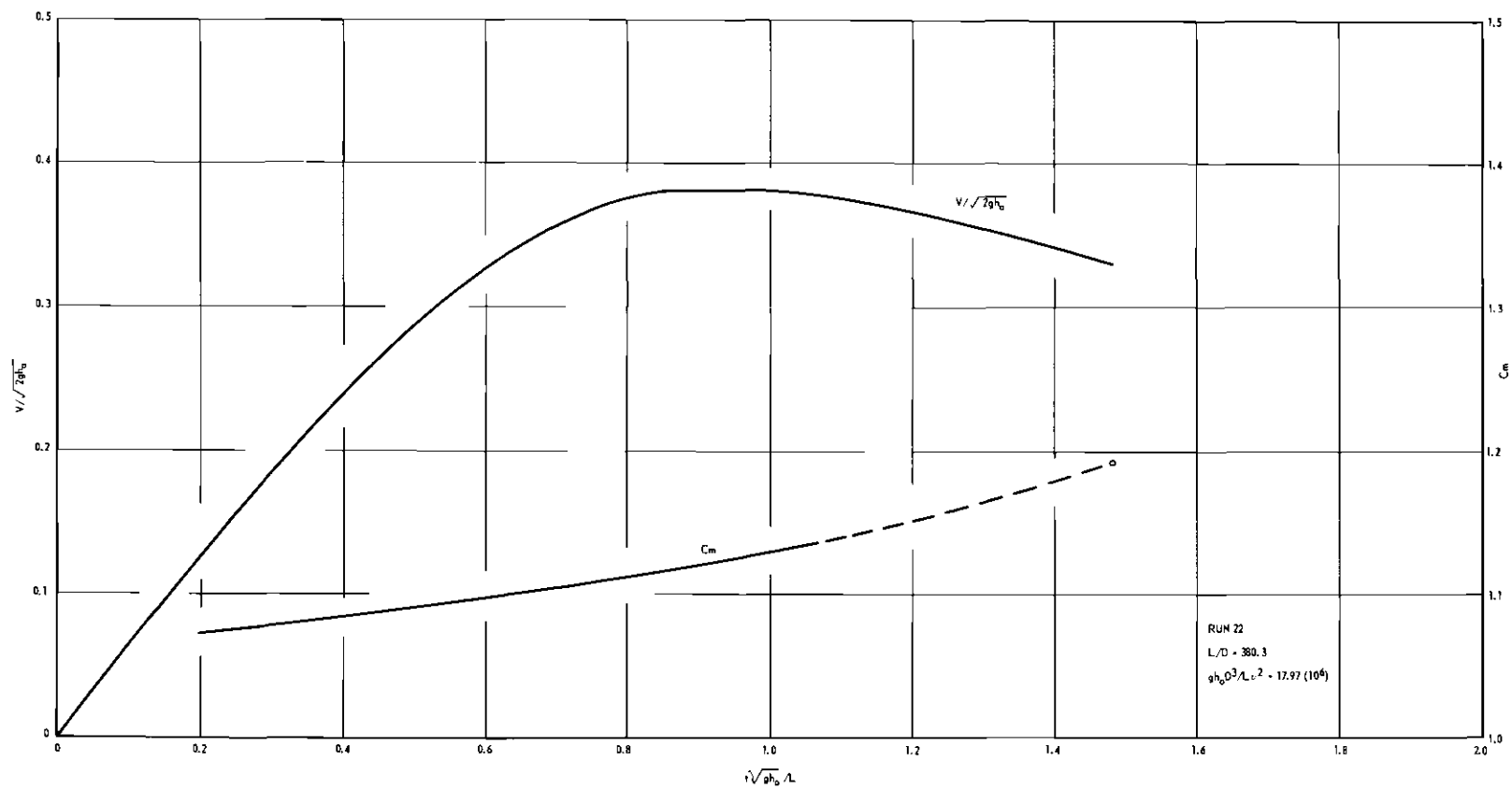Figure 16.   Fluid Element within the Pipe.
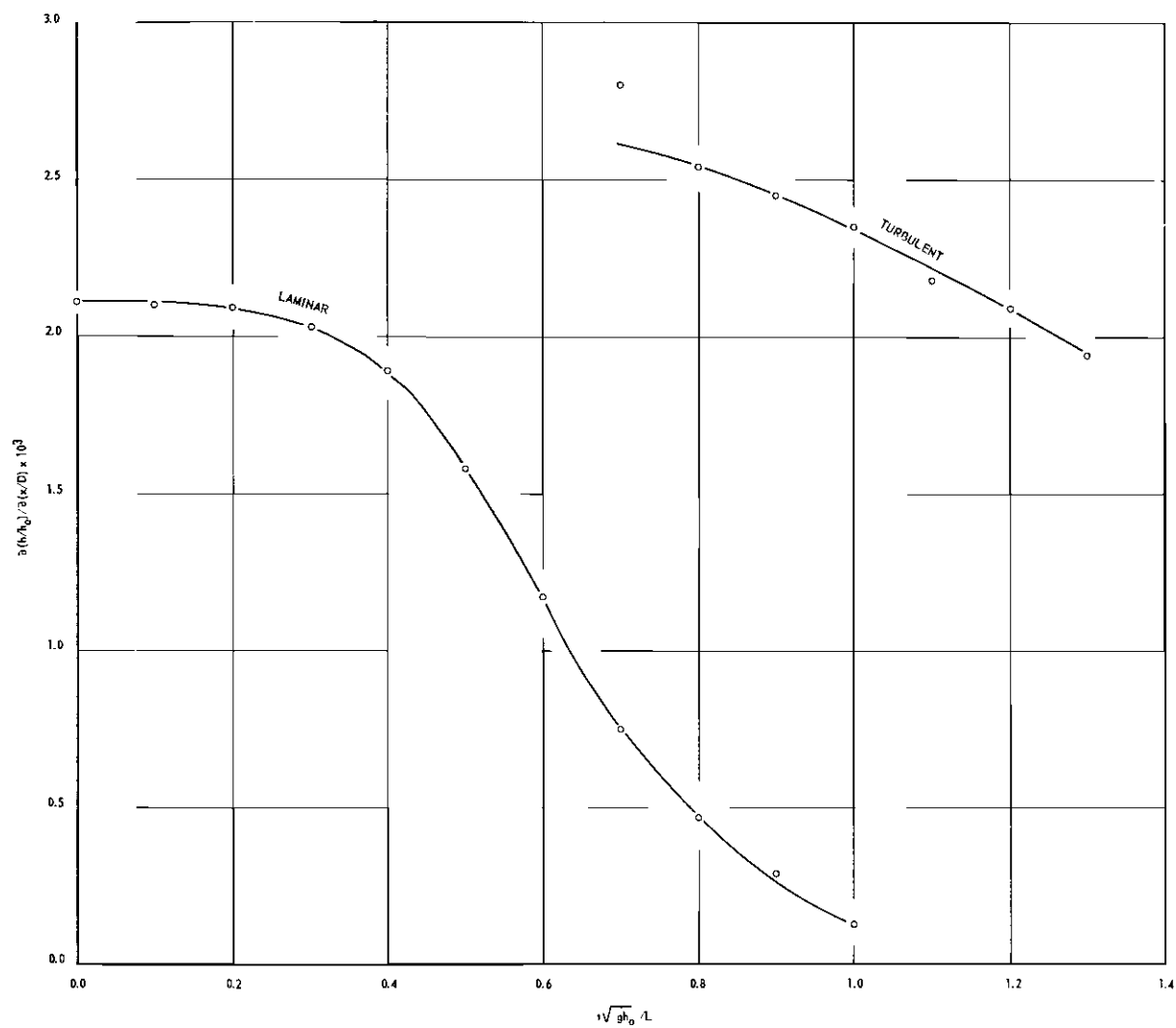
Figure 17. Temporal Variation of Piezometric Head Gradient for Run 29.
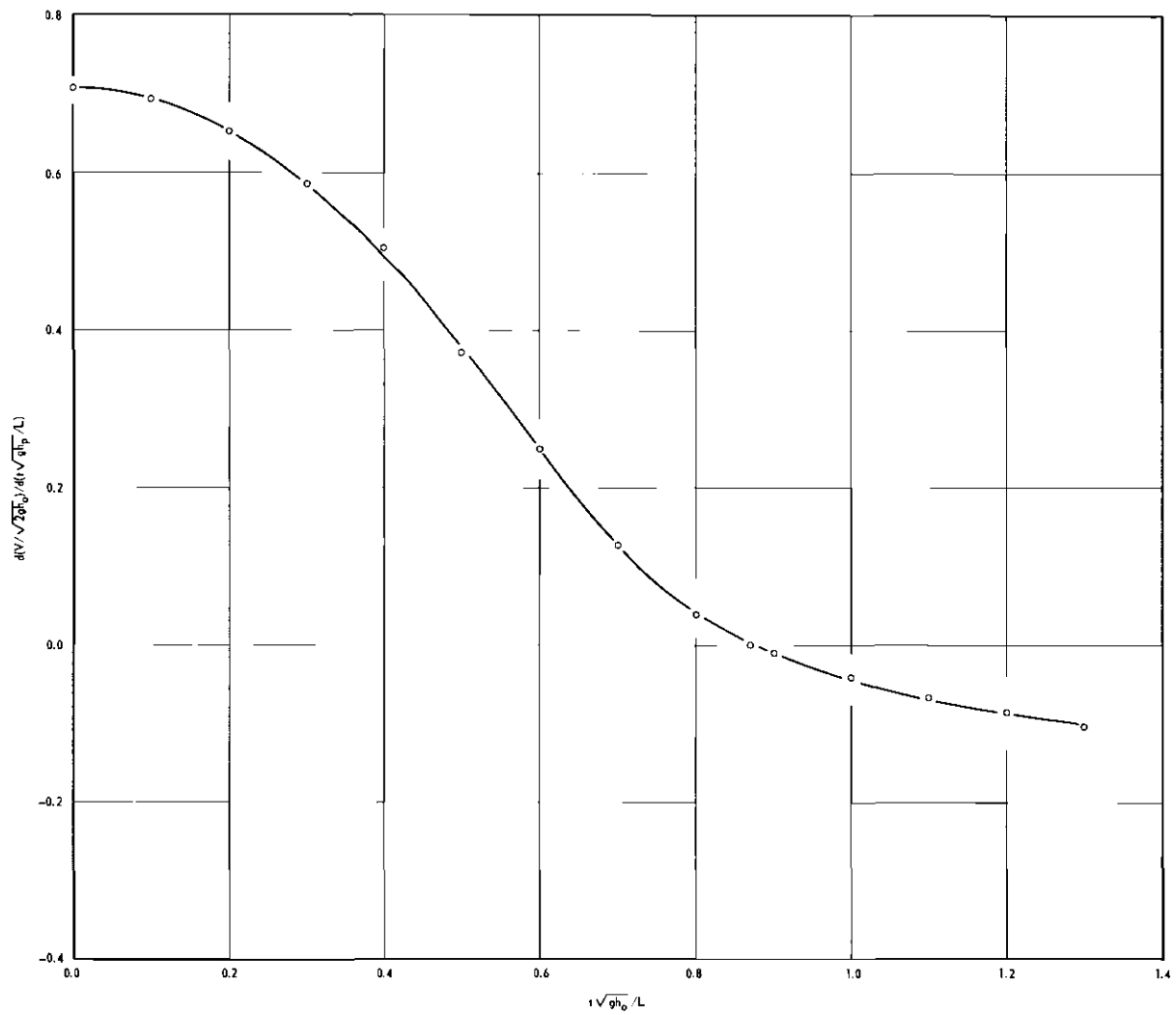
Figure 18. Temporal Variation of Dimensionless Fluid Acceleration for Run 29.
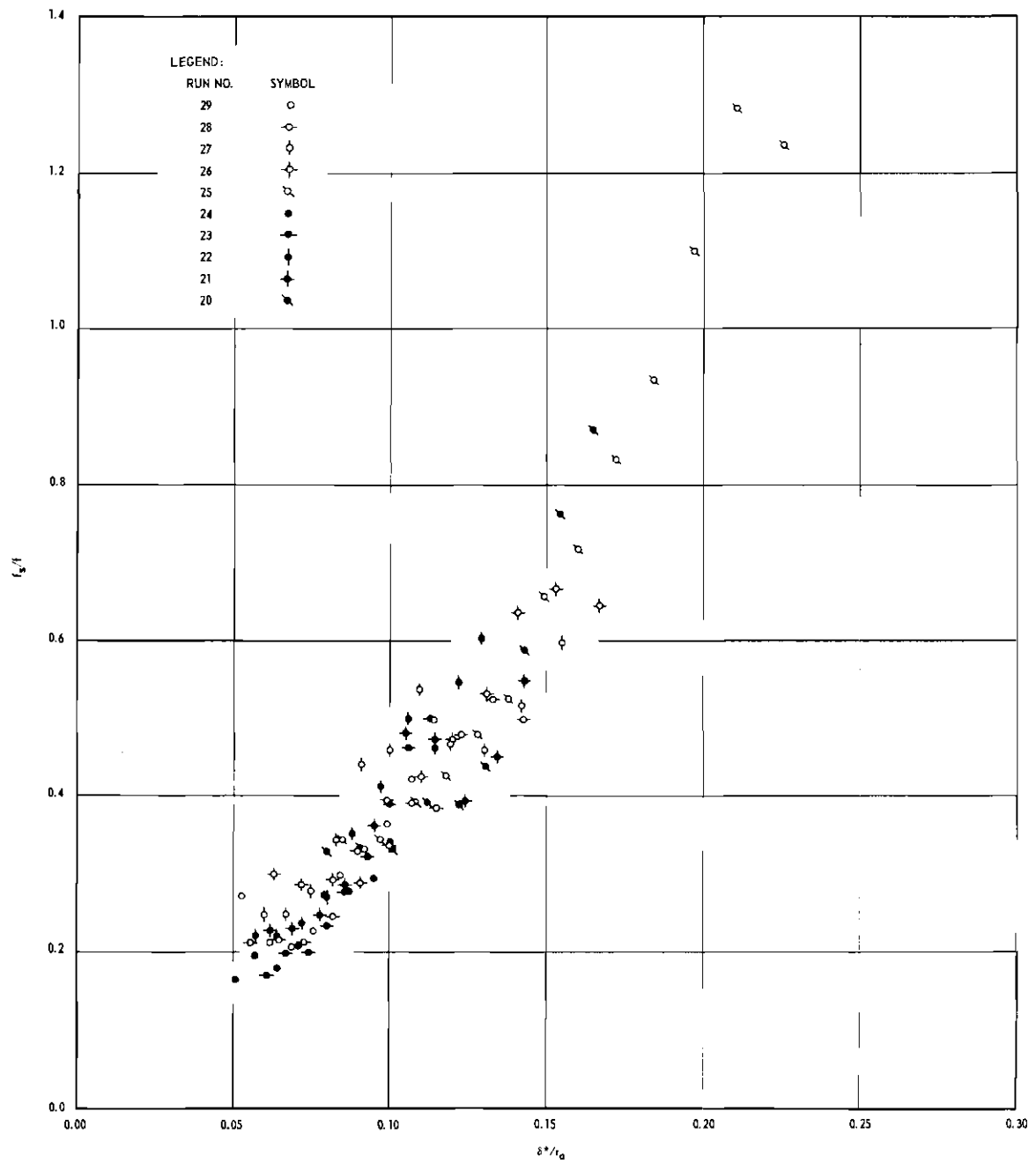
Figure 19.   Experimentally Determined Laminar Shear Results.

Figure 20. Mathematically Determined Laminar Shear Results from the
Solution of the Navier-Stokes Equations.

Figure 21. Experimentally Determined Turbulent Shear Results.

BIBLIOGRAPHY

Christopherson, D. G., et al. "Oscillatory Motion of a Fluid Along a Circular Tube," Proceedings of the Royal Society of London, Series A, Vol. 168, November, 1938, p. 351.

Clarion, C. "Sur l'amortissement des petites oscillations d'un liquide pesant et visqueux dans un tube en U," Comptes Rendus des Séances de l'Académie des Sciences, Vol. 230, 1950, p. 1926.
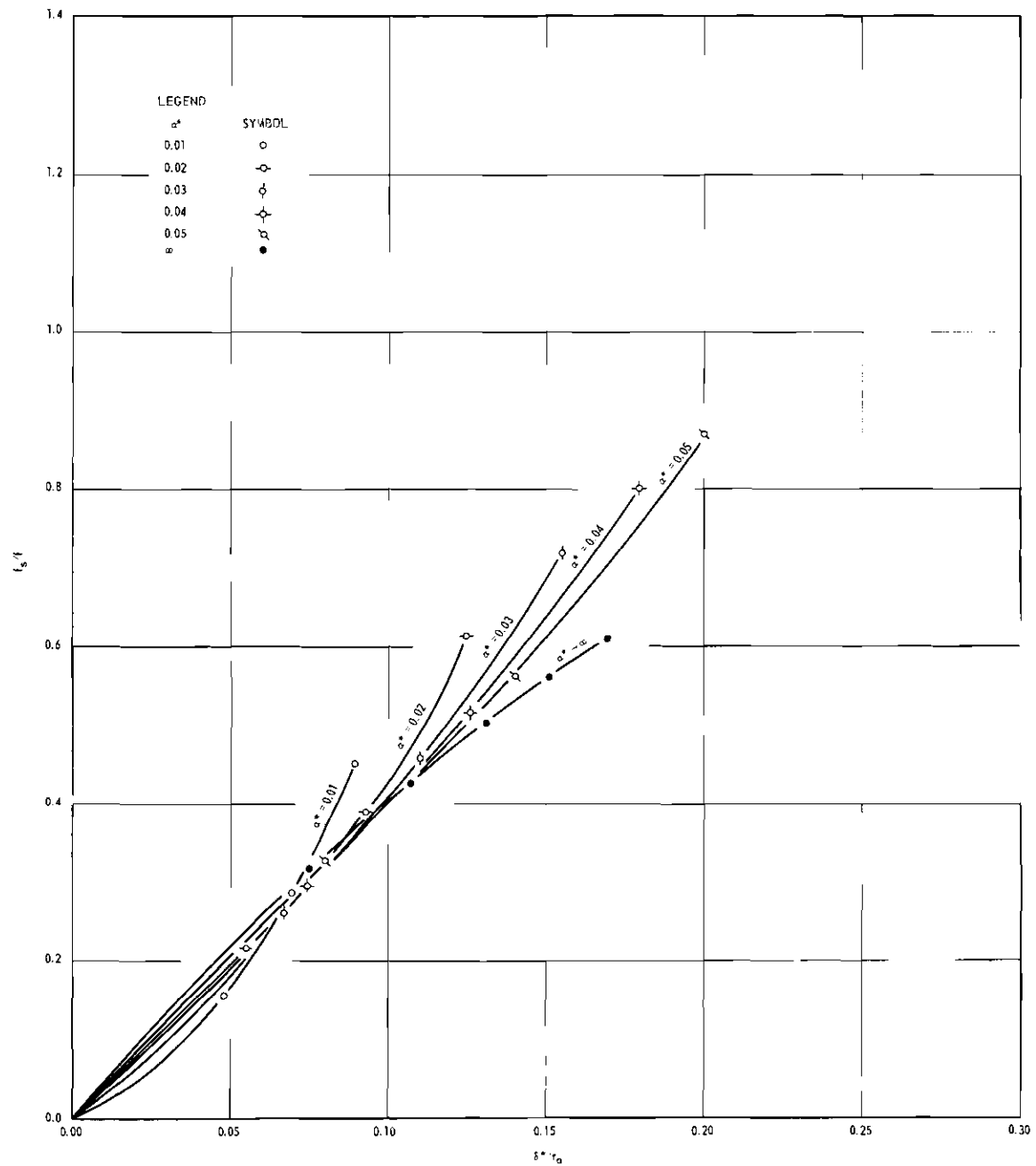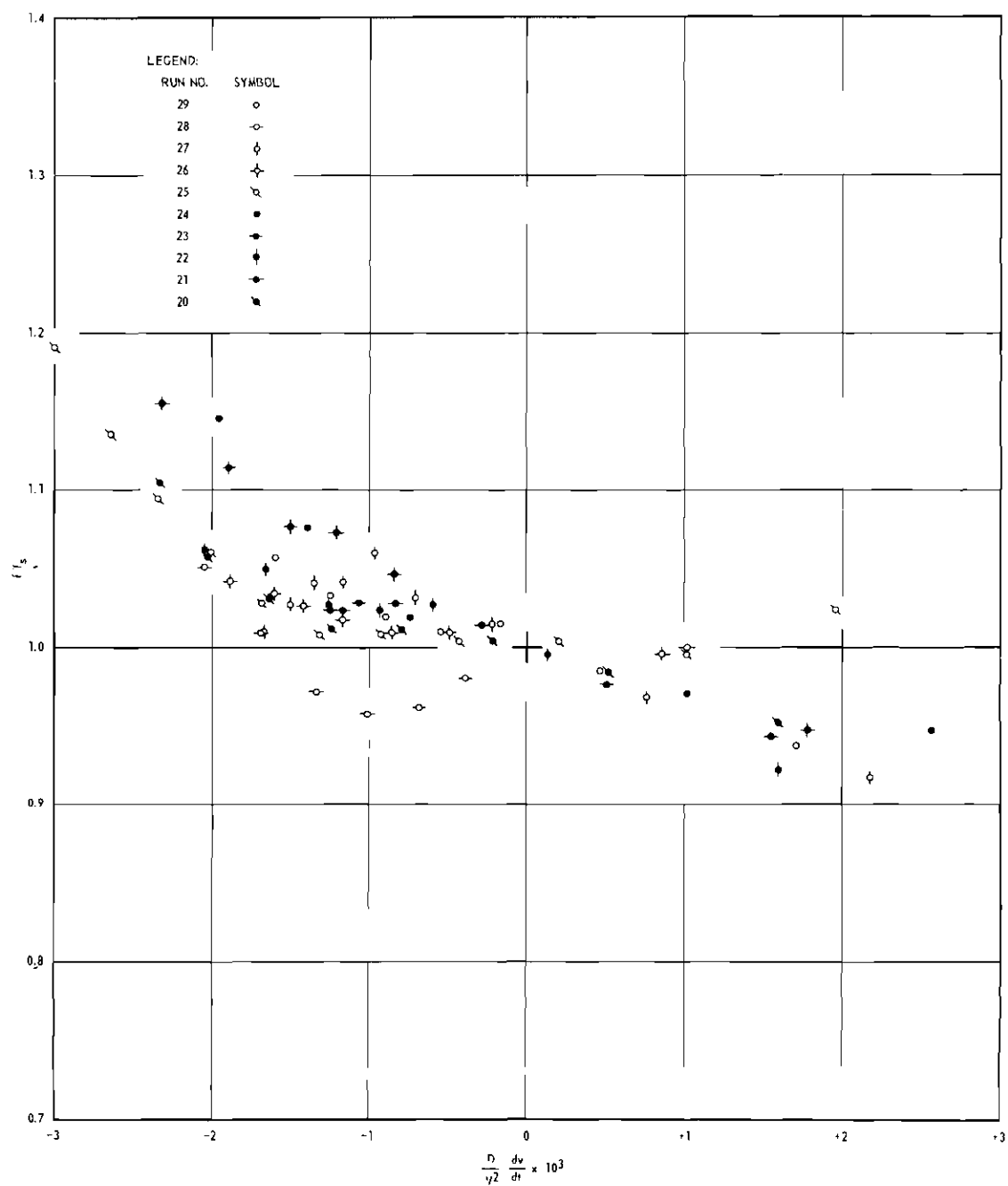
Crausse, E. "Contribution à l'étude expérimentale de phénomènes transitoires et de phénomènes périodiques se produisant dans les liquides en mouvement," Publication Scientifiques et Techniques du Ministère de l'Air, No. 95, 1936.

Daily, James W., and Deemer, Kenneth C. "The Unsteady-Flow Water Tunnel at the Massachusetts Institute of Technology," Transactions of the American Society of Mechanical Engineering, Vol. 76, January 1954, p. 87.

Goldstein, S. (editor). Modern Developments in Fluid Dynamics, Vol. I, Oxford: The Clarendon Press, 1938, p. 299-304.

Jones, D. B. "Measurement of Fluid Resistance in Oscillatory Unsteady Flow in a Smooth Pipe," Unpublished Master's thesis, State University of Iowa, August 1954, 54p.

Langhaar, Henry L. "Steady Flow in the Transition Length of a Straight Tube," Journal of Applied Mechanics, Vol. 9, No. 1, March, 1942, p. A55-A58.

Laufer, John. "The Structure of Turbulence in Fully Developed Pipe Flow," United States National Advisory Committee for Aeronautics, Report 1174, 1954.

Prandtl, L., and Tietjens, O. G. Applied Hydro- and Aeromechanics. Translated by J. P. Den Hartog. New York: The McGraw-Hill Book Company, 1934, p. 40-74.

Rich, George B. Hydraulic Transients. New York: The McGraw-Hill Book Company, 1951.

Sandborn, Virgil A. "Experimental Evaluation of Momentum Terms in Turbulent Pipe Flow," United States National Advisory Committee for Aeronautics, Technical Note 3266, January 1955.

Schlichting, H. Boundary Layer Theory. Translated by J. Kestin. New York: The McGraw-Hill Book Company, 1955.

Szymanski, Piotr. "Quelques solutions exactes des équations de l'hydrodynamique du fluide visqueux dans le cas d'un tube cylindrique," Journal de Mathématiques Pures et Appliquées, Series 9, Vol. 11, 1932, p. 67-107.

Valensi, J., and Clarion, C. "Mouvement oscillatoire d'un liquide visqueux et pesant dans un tube en U; photograhie du profil des déplacements; mise en évidence de la turbulence," Comptes Rendus des Séances de l'Académie des Sciences, Vol. 226, 1948, p. 554.

Yamada, H., and Taneda, S. "Note on the Liquid Motion in a U-tube," Reports of the Research Institute for Fluid Engineering, Kyushu University, Japan, Vol. VII, September, 1950, p. 1.

APPENDIX

TABLE I

TABULATED EXPERIMENTAL RESULTS OF LAMINAR SHEAR

Run No.	$t\sqrt{gh_o}/L$	$-\dfrac{\partial(h/h_o)}{\partial(x/D)}$	$\dfrac{V}{\sqrt{2gh_o}}$	$\dfrac{d(V/\sqrt{2gh_o})}{d(t\sqrt{gh_o}/L)}$	f	$\dfrac{\delta^*}{r_o}$
20	0.3	0.00257	0.185	0.55	0.0156	0.080
	0.4	0.00250	0.236	0.49	0.0121	0.091
	0.5	0.00236	0.282	0.42	0.0100	0.101
	0.6	0.00212	0.324	0.34	0.00748	0.112
	0.7	0.00176	0.355	0.24	0.00690	0.122
	0.8	0.00125	0.372	0.12	0.00580	0.133
	0.9	0.00076	0.379	0.04	0.00424	0.143
	1.0	0.00040	0.379	− 0.02	0.00327	0.154
	1.1	0.00019	0.376	− 0.06	0.00289	0.165
21	0.2	0.00261	0.125	0.60	0.0238	0.062
	0.3	0.00258	0.183	0.55	0.0159	0.069
	0.4	0.00246	0.235	0.49	0.0116	0.078
	0.5	0.00226	0.281	0.43	0.00836	0.086
	0.6	0.00197	0.321	0.37	0.00573	0.095
	0.7	0.00153	0.353	0.28	0.00395	0.105
	0.8	0.00105	0.375	0.14	0.00378	0.114
	0.9	0.00065	0.381	0.00	0.00448	0.124
	1.0	0.00034	0.377	− 0.06	0.00394	0.134
	1.1	0.00011	0.368	− 0.09	0.00331	0.143
22	0.2	0.00261	0.128	0.62	0.0194	0.057
	0.3	0.00255	0.186	0.56	0.0134	0.064
	0.4	0.00242	0.240	0.50	0.00967	0.072
	0.5	0.00218	0.287	0.43	0.00708	0.080
	0.6	0.00181	0.327	0.35	0.00476	0.088
	0.7	0.00136	0.355	0.24	0.00374	0.097
	0.8	0.00086	0.375	0.12	0.00293	0.106
	0.9	0.00049	0.382	0.01	0.00308	0.114
	1.0	0.00023	0.379	− 0.04	0.00264	0.122
	1.1	0.00008	0.374	− 0.07	0.00242	0.129
23	0.2	0.00262	0.127	0.61	0.0219	0.061
	0.3	0.00254	0.185	0.56	0.0129	0.067
	0.4	0.00239	0.238	0.49	0.0100	0.074
	0.5	0.00210	0.287	0.41	0.00707	0.080
	0.6	0.00167	0.325	0.30	0.00529	0.086
	0.7	0.00122	0.350	0.19	0.00418	0.093
	0.8	0.00085	0.364	0.11	0.00334	0.100
	0.9	0.00053	0.371	0.04	0.00276	0.106
	1.0	0.00028	0.372	− 0.02	0.00254	0.113

(continued)

TABLE I (continued)

TABULATED EXPERIMENTAL RESULTS OF LAMINAR SHEAR

Run No.	$t\sqrt{gh_o}/L$	$-\dfrac{\partial(h/h_o)}{\partial(x/D)}$	$\dfrac{V}{\sqrt{2gh_o}}$	$\dfrac{d(V/\sqrt{2gh_o})}{d(t\sqrt{gh_o}/L)}$	f	$\dfrac{\delta^*}{r_o}$
24	0.2	0.00262	0.133	0.61	0.0194	0.051
	0.3	0.00255	0.190	0.55	0.0114	0.057
	0.4	0.00239	0.241	0.49	0.00983	0.064
	0.5	0.00210	0.285	0.41	0.00716	0.071
	0.6	0.00162	0.321	0.30	0.00486	0.079
	0.7	0.00112	0.345	0.16	0.00445	0.087
	0.8	0.00077	0.356	0.07	0.00405	0.095
25	0.3	0.00206	0.182	0.54	0.0136	0.085
	0.4	0.00197	0.231	0.47	0.0107	0.097
	0.5	0.00182	0.275	0.41	0.00790	0.108
	0.6	0.00163	0.313	0.34	0.00633	0.118
	0.7	0.00139	0.343	0.26	0.00517	0.128
	0.8	0.00110	0.366	0.17	0.00441	0.138
	0.9	0.00079	0.379	0.10	0.00340	0.149
	1.0	0.00051	0.382	0.02	0.00308	0.160
	1.1	0.00027	0.382	− 0.04	0.00267	0.172
	1.2	0.00007	0.375	− 0.09	0.00243	0.184
	1.3	− 0.00008	0.363	− 0.12	0.00212	0.197
	1.4	− 0.00019	0.349	− 0.14	0.00188	0.211
	1.5	− 0.00022	0.334	− 0.15	0.00205	0.226
26	0.2	0.00208	0.130	0.61	0.0153	0.063
	0.3	0.00204	0.190	0.55	0.0111	0.072
	0.4	0.00192	0.238	0.48	0.00860	0.082
	0.5	0.00171	0.279	0.38	0.00744	0.091
	0.6	0.00140	0.315	0.28	0.00566	0.100
	0.7	0.00099	0.341	0.17	0.00414	0.110
	0.8	0.00065	0.349	0.07	0.00361	0.120
	0.9	0.00040	0.353	0.00	0.00320	0.131
	1.0	0.00021	0.349	− 0.04	0.00270	0.141
	1.1	0.00010	0.343	− 0.07	0.00263	0.153
	1.2	0.00004	0.335	− 0.09	0.00277	0.167
27	0.2	0.00208	0.129	0.61	0.0153	0.060
	0.3	0.00200	0.181	0.55	0.0109	0.067
	0.4	0.00184	0.235	0.48	0.00746	0.075
	0.5	0.00159	0.281	0.40	0.00506	0.083
	0.6	0.00124	0.316	0.30	0.00350	0.091
	0.7	0.00087	0.339	0.17	0.00313	0.100
	0.8	0.00050	0.352	0.06	0.00258	0.109

(continued)

TABLE I (continued)

TABULATED EXPERIMENTAL RESULTS OF LAMINAR SHEAR

Run No.	$t\sqrt{gh_o}/L$	$-\dfrac{\partial(h/h_o)}{\partial(x/D)}$	$\dfrac{V}{\sqrt{2gh_o}}$	$\dfrac{d(V/\sqrt{2gh_o})}{d(t\sqrt{gh_o}/L)}$	f	$\dfrac{\delta^*}{r_o}$
27	0.9	0.00031	0.353	$-$ 0.02	0.00296	0.119
	1.0	0.00019	0.350	$-$ 0.06	0.00304	0.130
	1.1	0.00008	0.341	$-$ 0.08	0.00276	0.142
	1.2	0.00000	0.333	$-$ 0.09	0.00246	0.155
28	0.2	0.00207	0.128	0.61	0.0156	0.056
	0.3	0.00200	0.185	0.55	0.0106	0.065
	0.4	0.00187	0.237	0.47	0.00840	0.073
	0.5	0.00161	0.282	0.38	0.00607	0.082
	0.6	0.00124	0.314	0.28	0.00408	0.090
	0.7	0.00090	0.338	0.18	0.00316	0.099
	0.8	0.00062	0.351	0.08	0.00309	0.107
	0.9	0.00039	0.355	0.00	0.00309	0.115
	1.0	0.00022	0.353	$-$ 0.03	0.00250	0.123
	1.1	0.00010	0.349	$-$ 0.06	0.00230	0.133
	1.2	0.00005	0.342	$-$ 0.08	0.00248	0.200
29	0.2	0.00209	0.131	0.64	0.0106	0.053
	0.3	0.00203	0.187	0.57	0.0094	0.062
	0.4	0.00189	0.237	0.49	0.0077	0.069
	0.5	0.00158	0.282	0.38	0.0057	0.076
	0.6	0.00114	0.314	0.25	0.0040	0.084
	0.7	0.00075	0.331	0.13	0.0033	0.092
	0.8	0.00046	0.338	0.04	0.0030	0.099
	0.9	0.00027	0.339	$-$ 0.01	0.0026	0.107
	1.0	0.00013	0.337	$-$ 0.04	0.0022	0.114

TABLE II

TABULATED EXPERIMENTAL RESULTS OF TURBULENT SHEAR

Run No.	$t\sqrt{gh_o}/L$	$-\dfrac{\partial(h/h_o)}{\partial(x/D)}$	$\dfrac{V}{\sqrt{2gh_o}}$	$\dfrac{d(V/\sqrt{2gh_o})}{d(t\sqrt{gh_o}/L)}$	f
20	0.8	0.00345	0.372	0.118	0.0218
	0.9	0.00337	0.379	0.040	0.0224
	0.97	0.00328	0.380	0.000	0.0228
	1.0	0.00324	0.379	− 0.017	0.0229
	1.1	0.00305	0.376	− 0.060	0.0232
	1.2	0.00281	0.368	− 0.090	0.0233
	1.3	0.00262	0.357	− 0.115	0.0240
	1.4	0.00248	0.345	− 0.130	0.0249
	1.5	0.00239	0.332	− 0.138	0.0264
21	0.8	0.00328	0.375	0.135	0.0197
	0.9	0.00315	0.381	0.000	0.0217
	1.0	0.00301	0.376	− 0.064	0.0230
	1.1	0.00287	0.369	− 0.088	0.0235
	1.2	0.00272	0.360	− 0.105	0.0239
	1.3	0.00255	0.348	− 0.123	0.0249
	1.4	0.00240	0.335	− 0.140	0.0261
22	0.8	0.00333	0.374	0.120	0.0206
	0.9	0.00326	0.382	0.010	0.0221
	0.91	0.00324	0.382	0.000	0.0222
	1.0	0.00311	0.378	− 0.045	0.0229
	1.1	0.00293	0.374	− 0.070	0.0228
	1.2	0.00275	0.366	− 0.091	0.0231
	1.3	0.00256	0.355	− 0.112	0.0237
	1.4	0.00237	0.343	− 0.130	0.0242
23	0.8	0.00309	0.364	0.110	0.0203
	0.9	0.00303	0.372	0.038	0.0209
	0.96	0.00297	0.373	0.000	0.0214
	1.0	0.00292	0.372	− 0.021	0.0217
	1.1	0.00276	0.367	− 0.060	0.0221
	1.2	0.00260	0.360	− 0.075	0.0222
	1.3	0.00246	0.352	− 0.078	0.0222
	1.4	0.00235	0.345	− 0.080	0.0223
24	0.7	0.00302	0.345	0.165	0.0203
	0.8	0.00289	0.356	0.070	0.0207
	0.9	0.00274	0.359	0.000	0.0212
	1.0	0.00257	0.355	− 0.050	0.0217
	1.1	0.00245	0.348	− 0.090	0.0230
	1.2	0.00235	0.337	− 0.120	0.0246
25	0.8	0.00366	0.364	0.175	0.0238
	0.9	0.00356	0.378	0.097	0.0229
	1.0	0.00342	0.382	0.020	0.0230

(continued)

TABLE II (continued)

TABULATED EXPERIMENTAL RESULTS OF TURBULENT SHEAR

Run No.	$t\sqrt{gh_o}/L$	$-\dfrac{\partial(h/h_o)}{\partial(x/D)}$	$\dfrac{V}{\sqrt{2gh_o}}$	$\dfrac{d(V/\sqrt{2gh_o})}{d(t\sqrt{gh_o}/L)}$	f
25	1.03	0.00337	0.383	0.000	0.0229
	1.1	0.00323	0.382	− 0.042	0.0230
	1.2	0.00309	0.375	− 0.088	0.0232
	1.3	0.00278	0.363	− 0.118	0.0237
	1.4	0.00256	0.350	− 0.139	0.0241
	1.5	0.00237	0.335	− 0.151	0.0252
	1.6	0.00221	0.320	− 0.160	0.0264
	1.7	0.00206	0.304	− 0.163	0.0277
	1.8	0.00194	0.287	− 0.165	0.0296
26	0.8	0.00300	0.350	0.071	0.0227
	0.9	0.00284	0.353	0.000	0.0227
	1.0	0.00269	0.349	− 0.040	0.0230
	1.1	0.00253	0.343	− 0.068	0.0231
	1.2	0.00237	0.335	− 0.088	0.0235
	1.3	0.00222	0.325	− 0.101	0.0238
	1.4	0.00207	0.315	− 0.110	0.0242
	1.5	0.00191	0.303	− 0.116	0.0246
27	0.7	0.00296	0.340	0.170	0.0211
	0.8	0.00288	0.351	0.063	0.0219
	0.87	0.00282	0.353	0.000	0.0226
	0.9	0.00279	0.352	− 0.018	0.0229
	1.0	0.00269	0.349	− 0.058	0.0234
	1.1	0.00256	0.341	− 0.076	0.0241
	1.2	0.00241	0.334	− 0.088	0.0238
	1.3	0.00225	0.325	− 0.096	0.0240
	1.4	0.00207	0.315	− 0.100	0.0239
	1.5	0.00187	0.304	− 0.103	0.0237
28	0.8	0.00305	0.352	0.085	0.0226
	0.9	0.00285	0.355	0.000	0.0226
	1.0	0.00267	0.353	− 0.032	0.0222
	1.1	0.00250	0.349	− 0.056	0.0219
	1.2	0.00235	0.343	− 0.080	0.0219
	1.3	0.00221	0.334	− 0.100	0.0224
	1.4	0.00208	0.323	− 0.118	0.0234
	1.5	0.00196	0.310	− 0.132	0.0245
29	0.7	0.00261	0.332	0.127	0.0203
	0.8	0.00254	0.338	0.039	0.0212
	0.87	0.00248	0.340	0.000	0.0214
	0.9	0.00245	0.339	− 0.013	0.0217
	1.0	0.00234	0.337	− 0.042	0.0217
	1.1	0.00222	0.332	− 0.067	0.0220
	1.2	0.00209	0.324	− 0.088	0.0224
	1.3	0.00194	0.313	− 0.105	0.0230
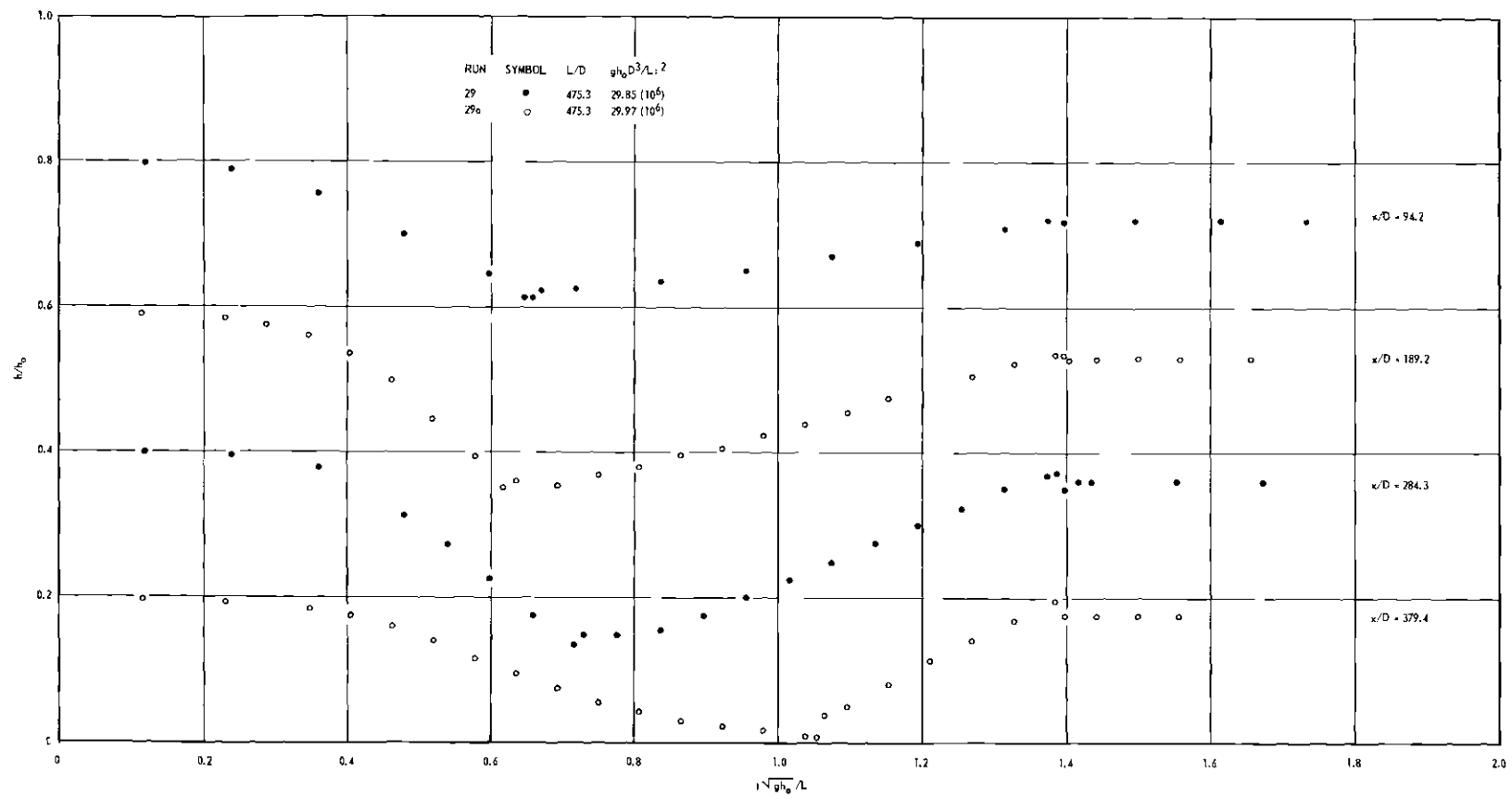
Figure 1A.   Pressure-time Data of Run 29.
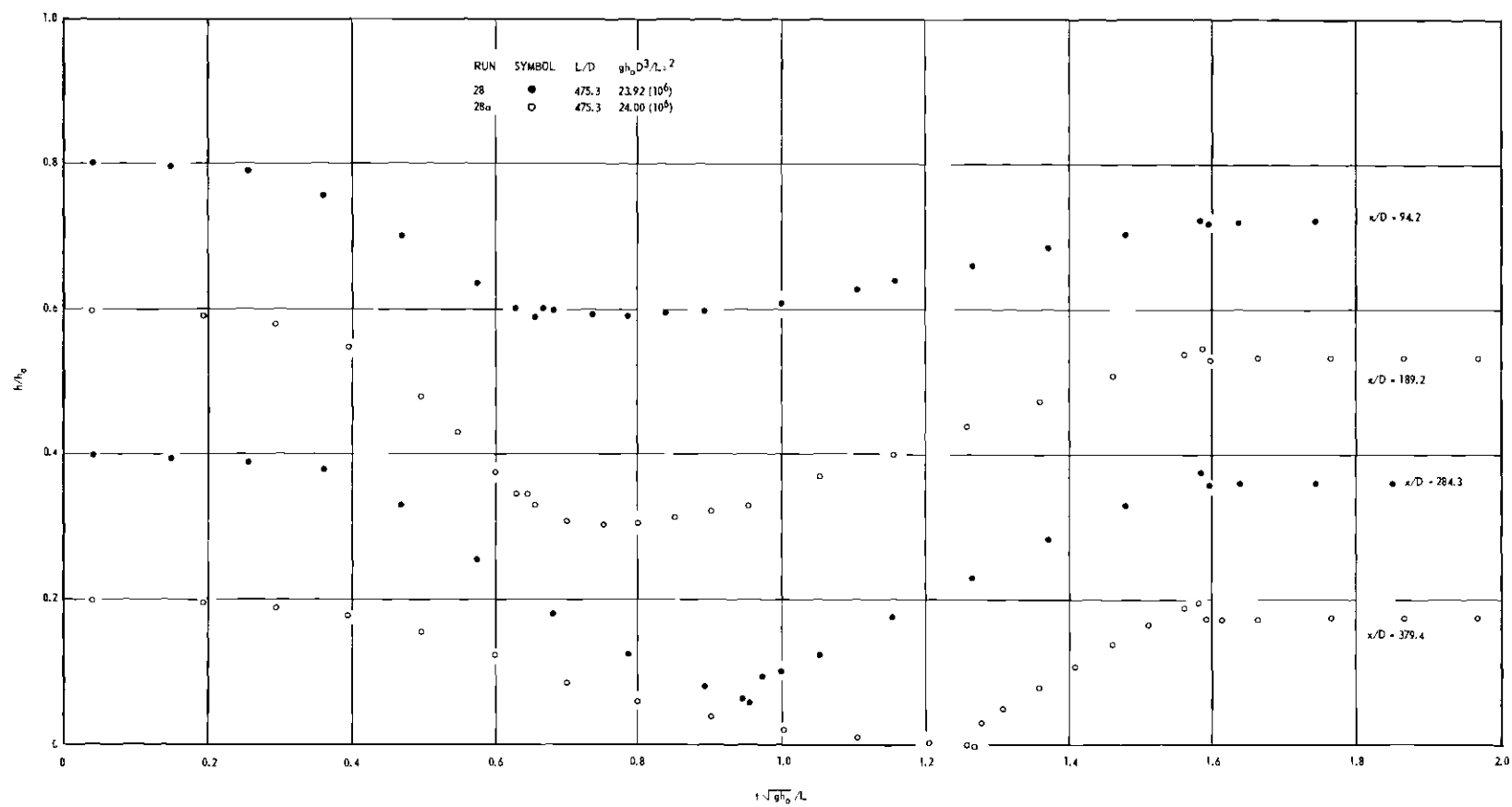
Figure 2A.   Pressure-time Data of Run 28.

57
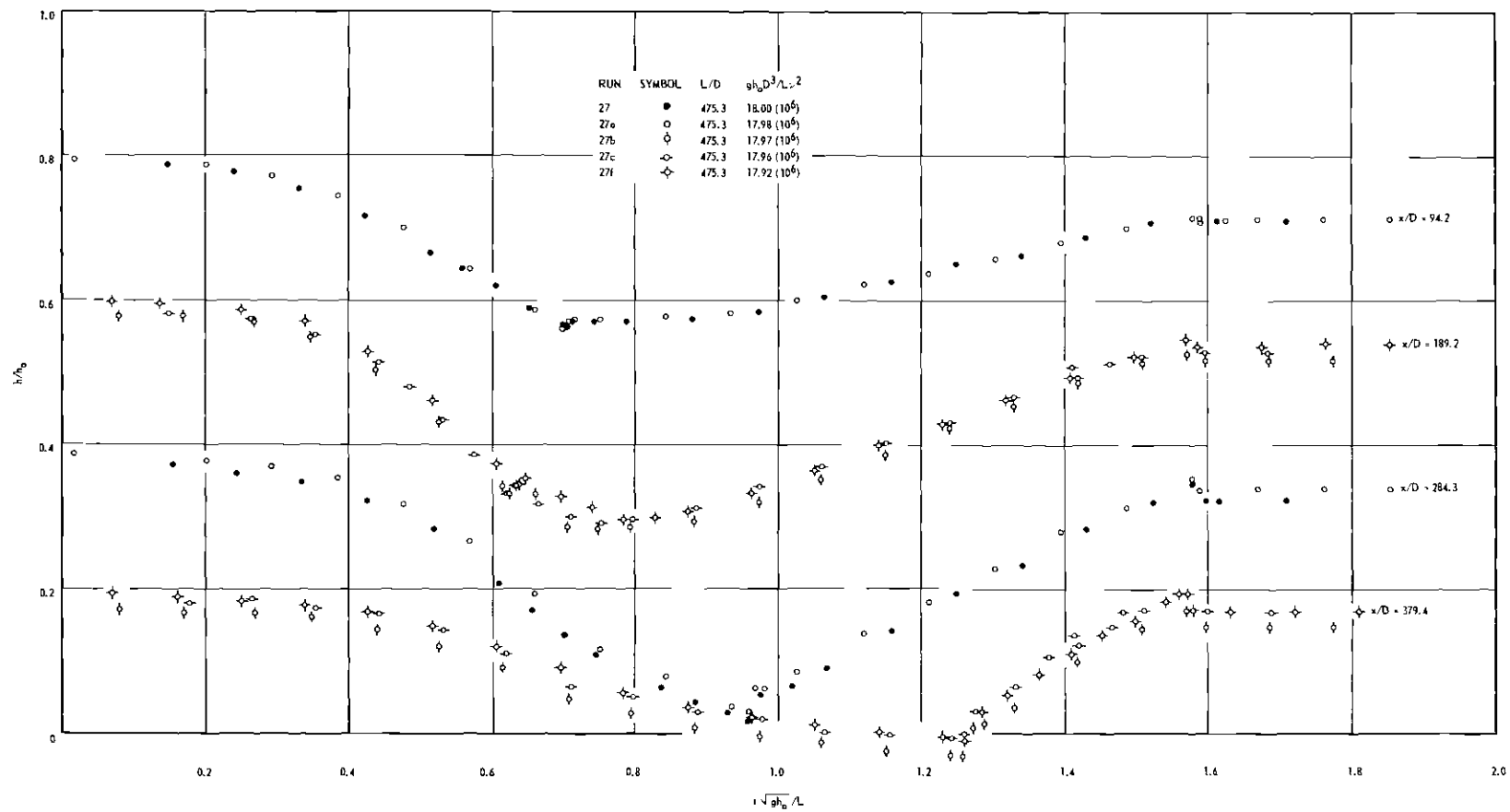
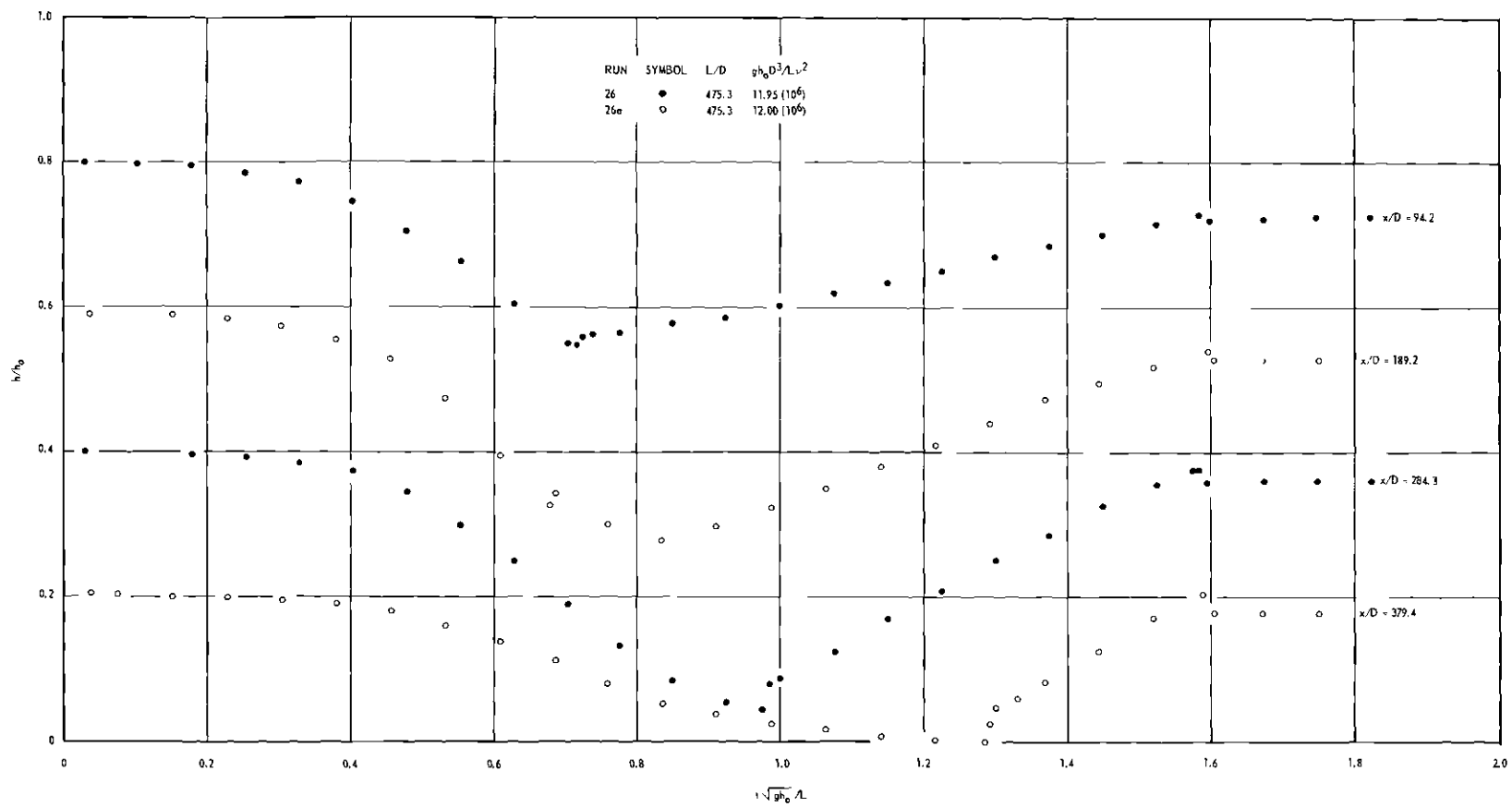Figure 3A.   Pressure-time Data of Run 27.
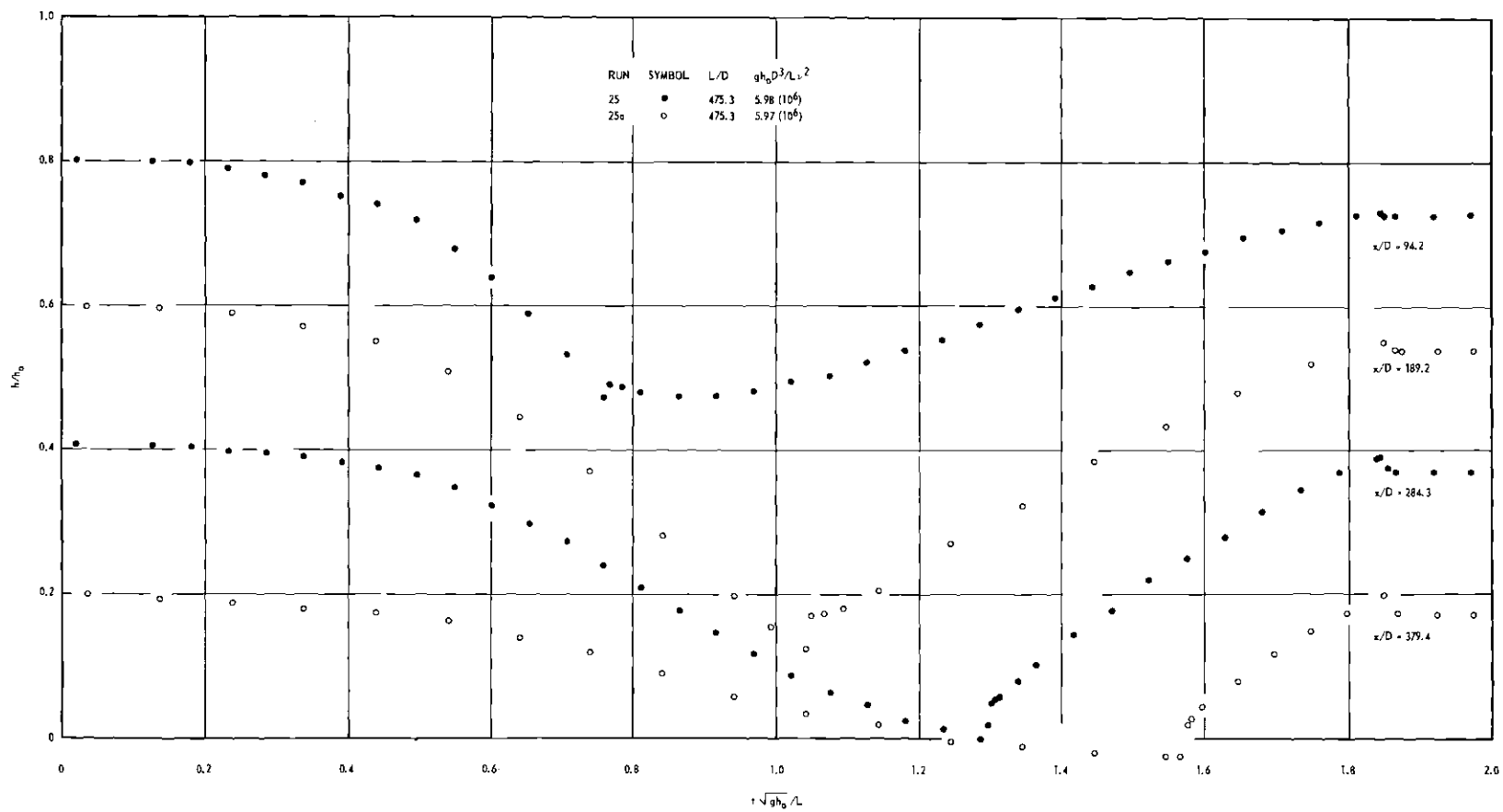
Figure 4A. Pressure-time Data of Run 26.

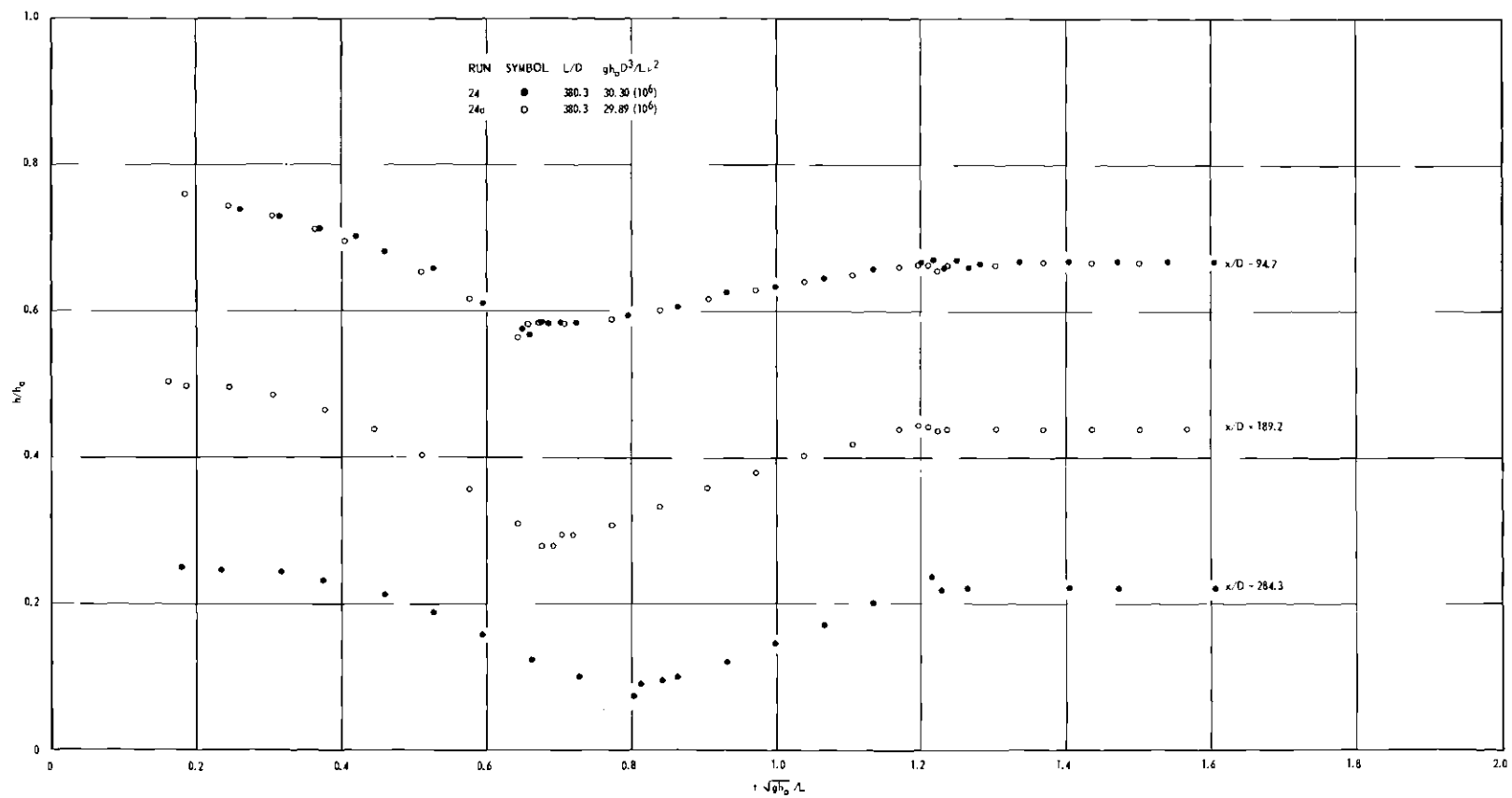Figure 5A.   Pressure-time Data of Run 25.
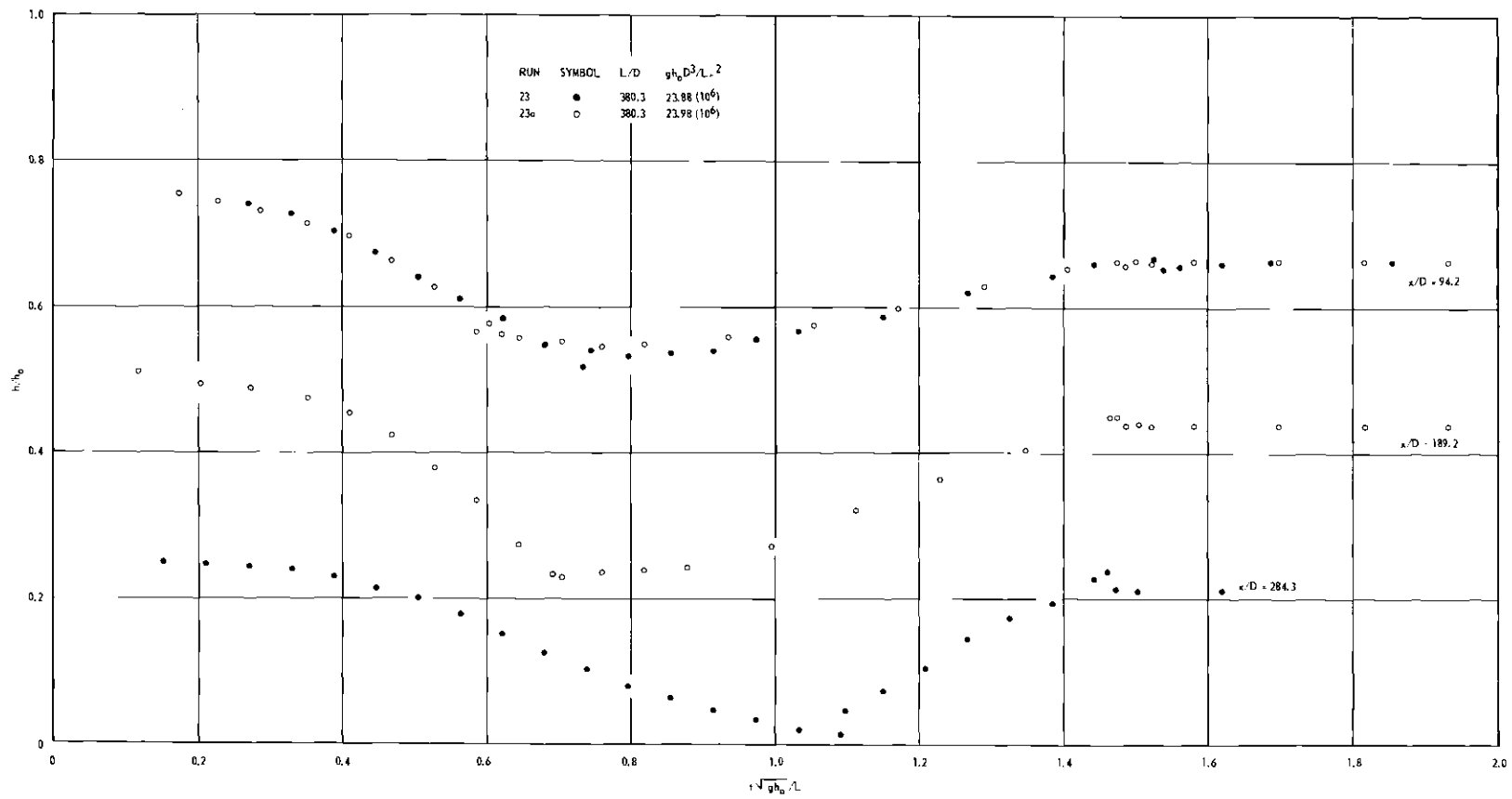
Figure 6A. Pressure-time Data of Run 24.
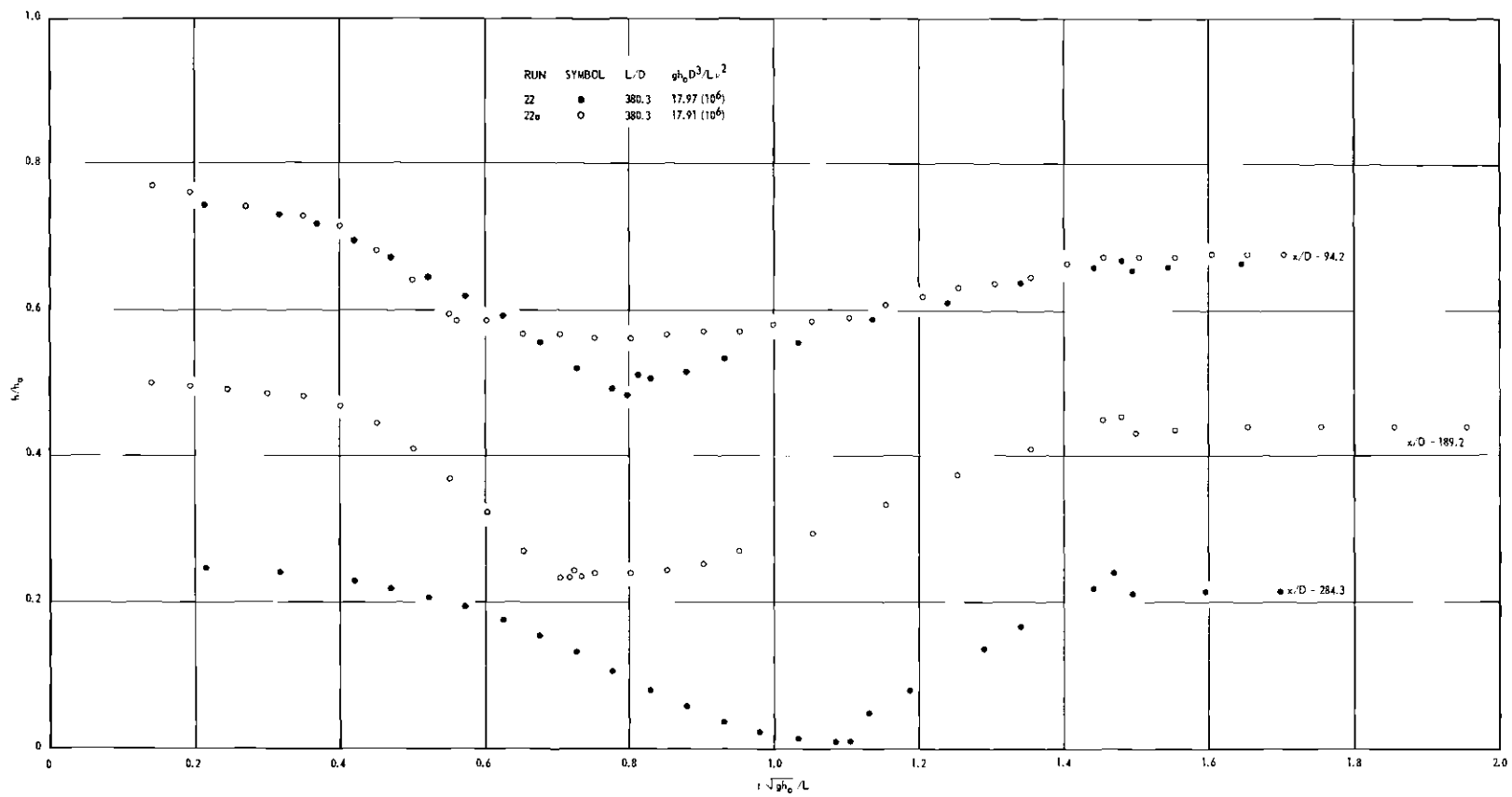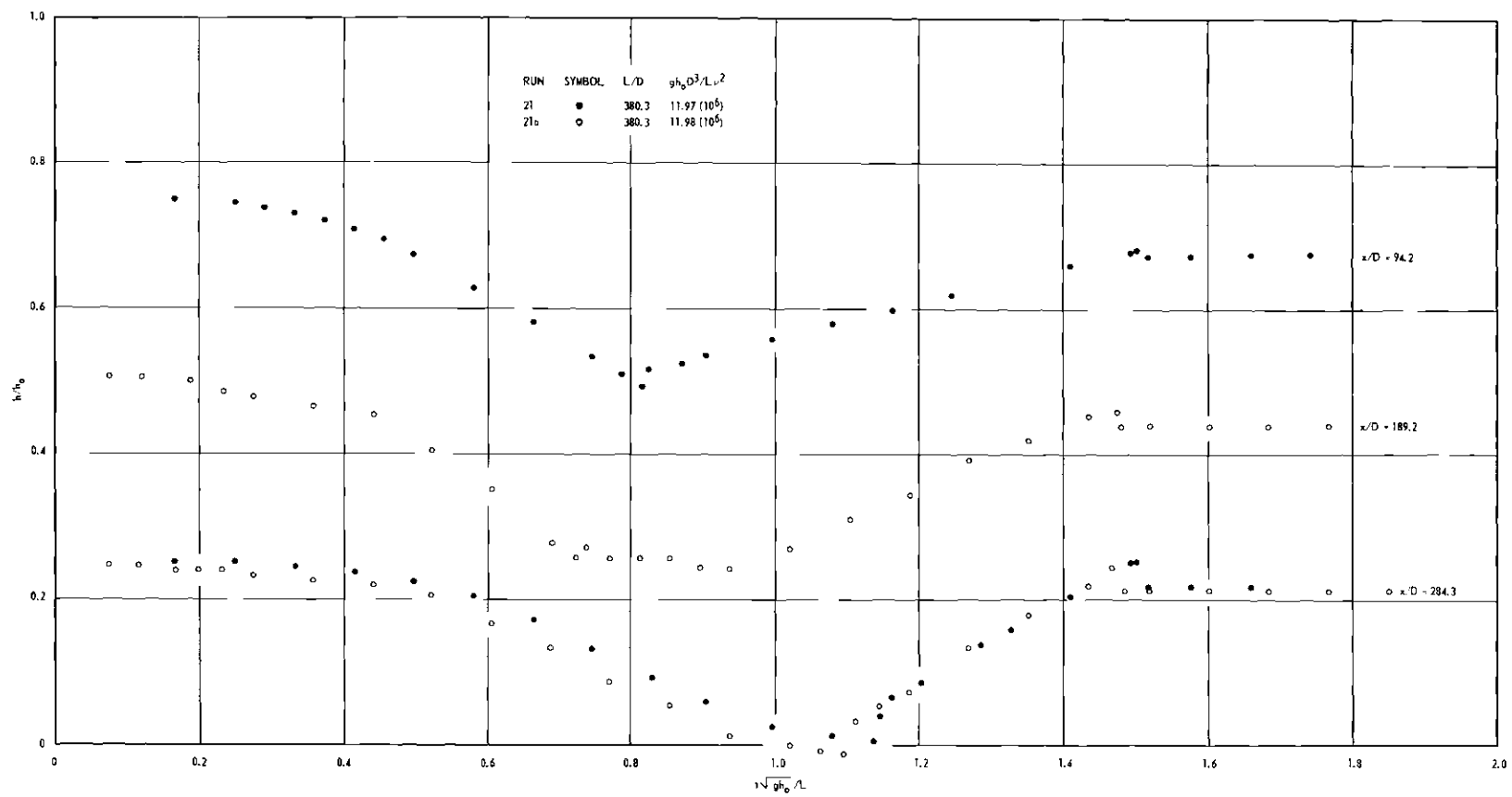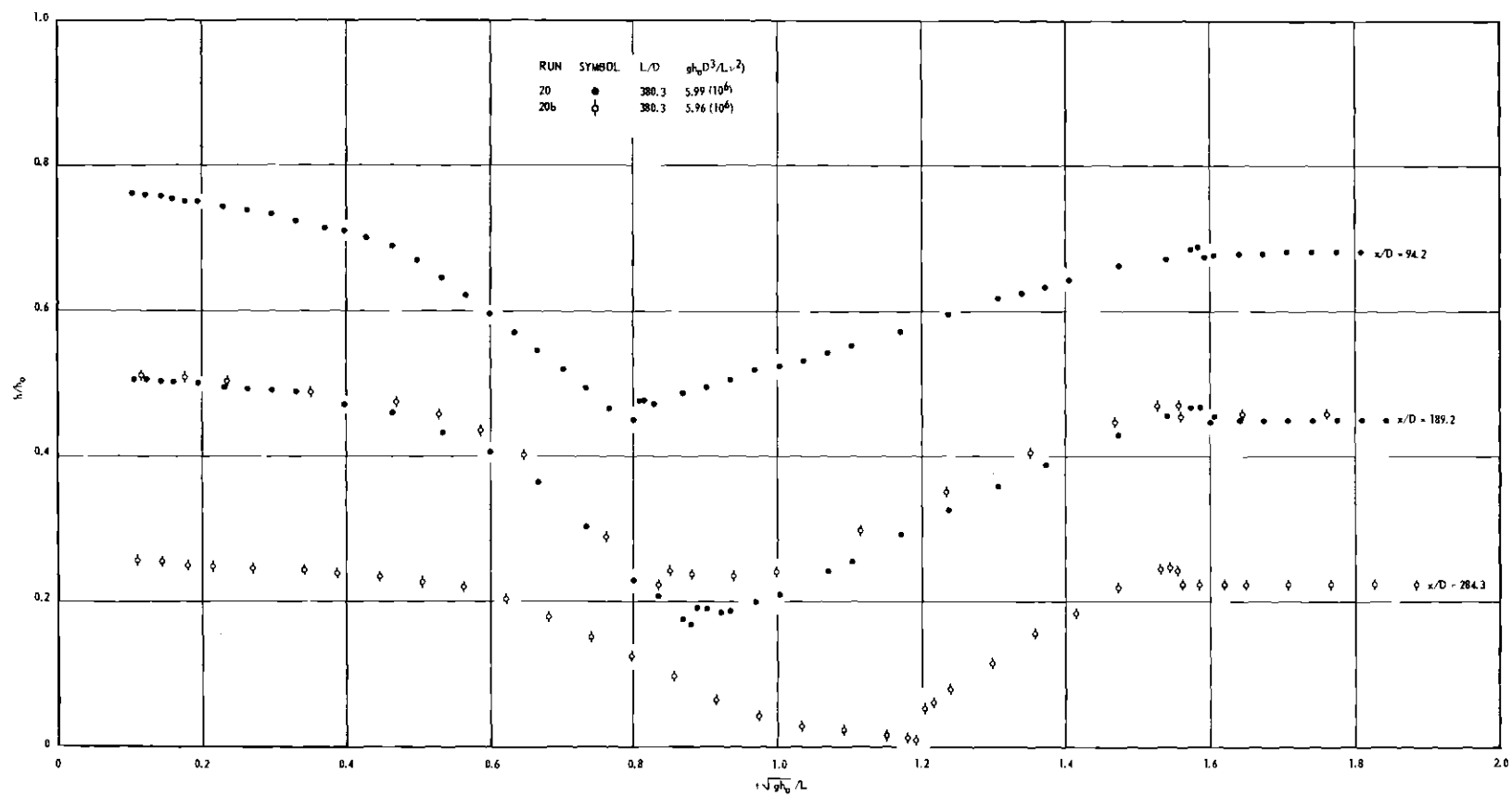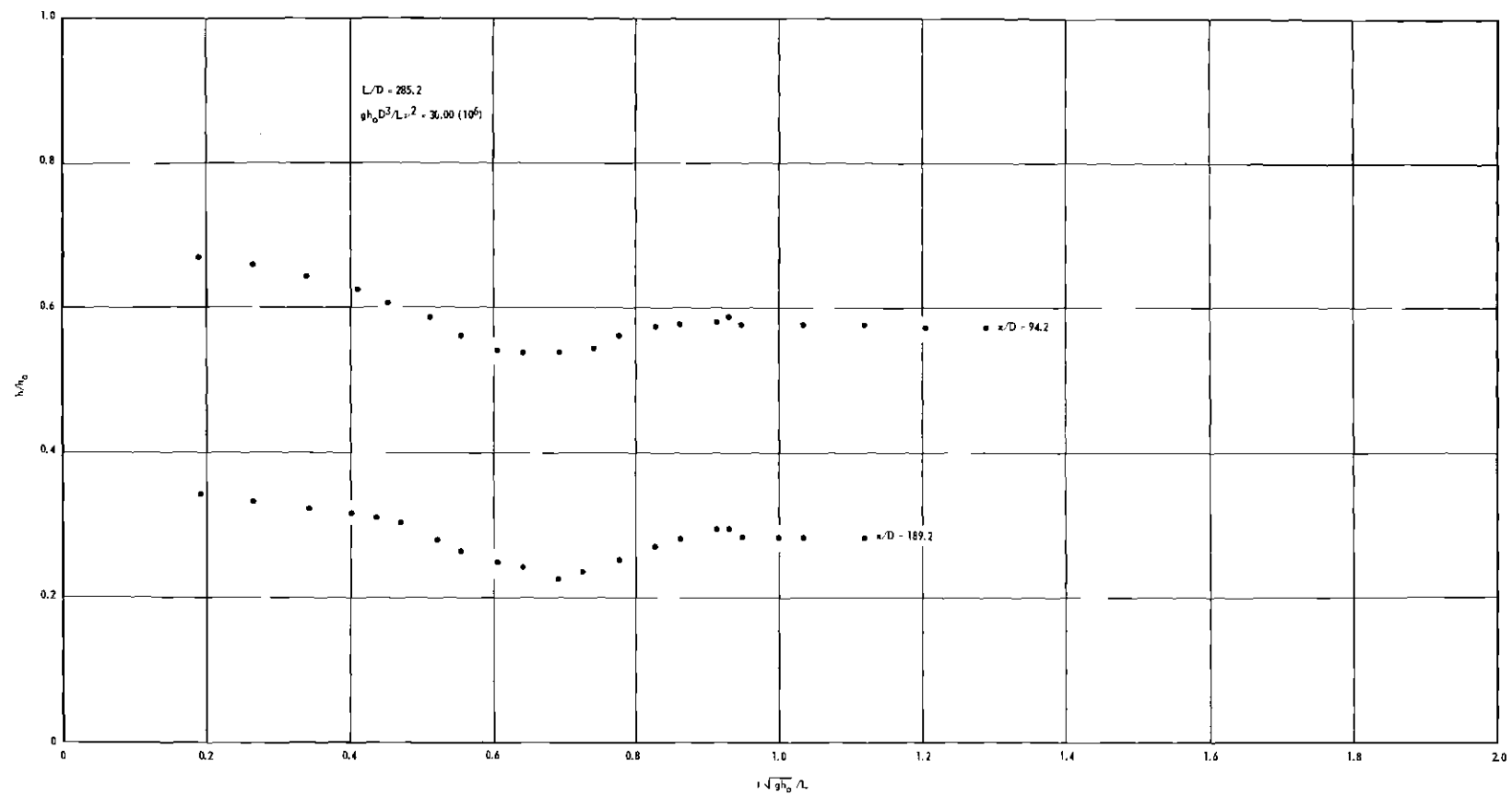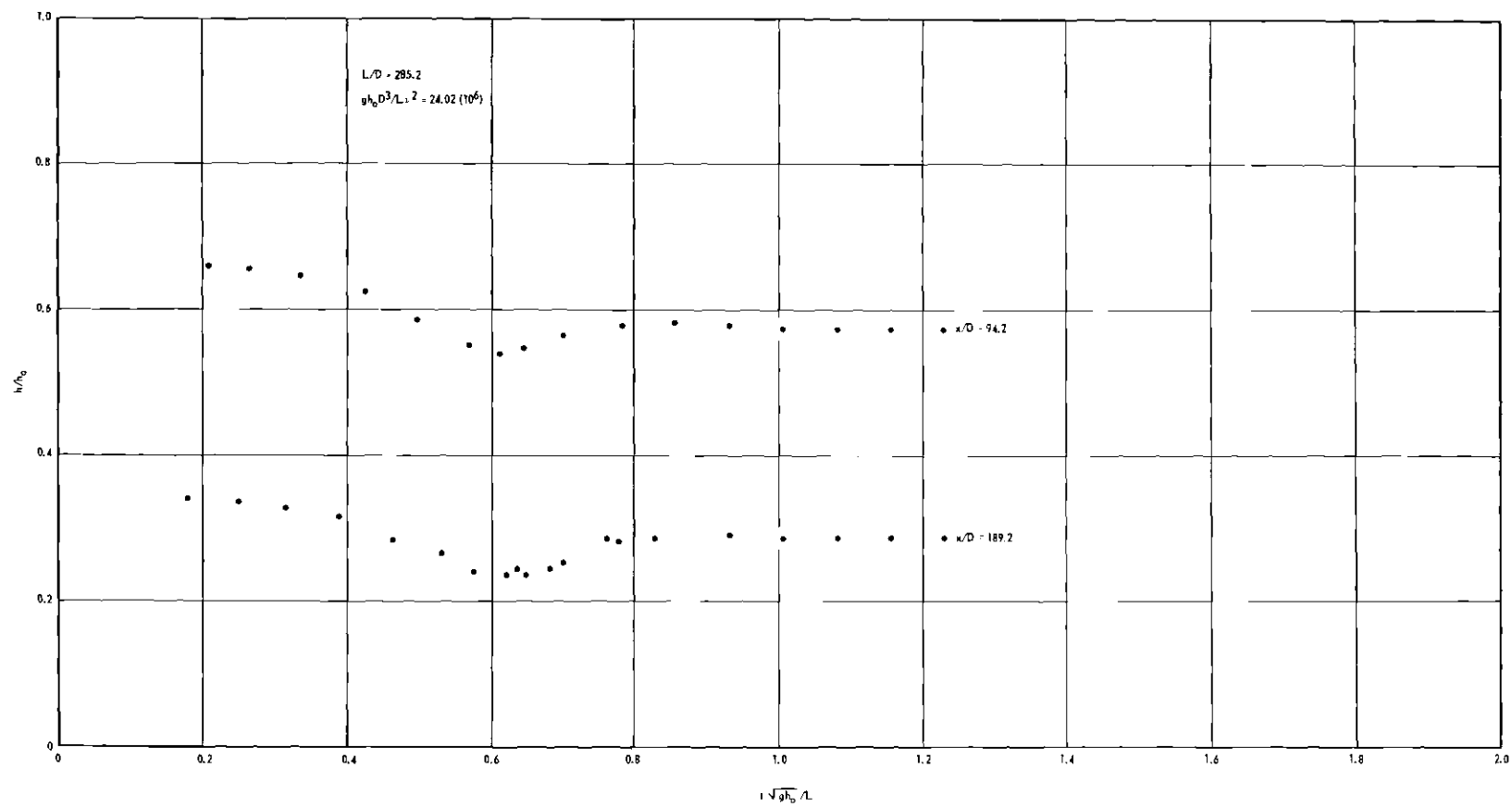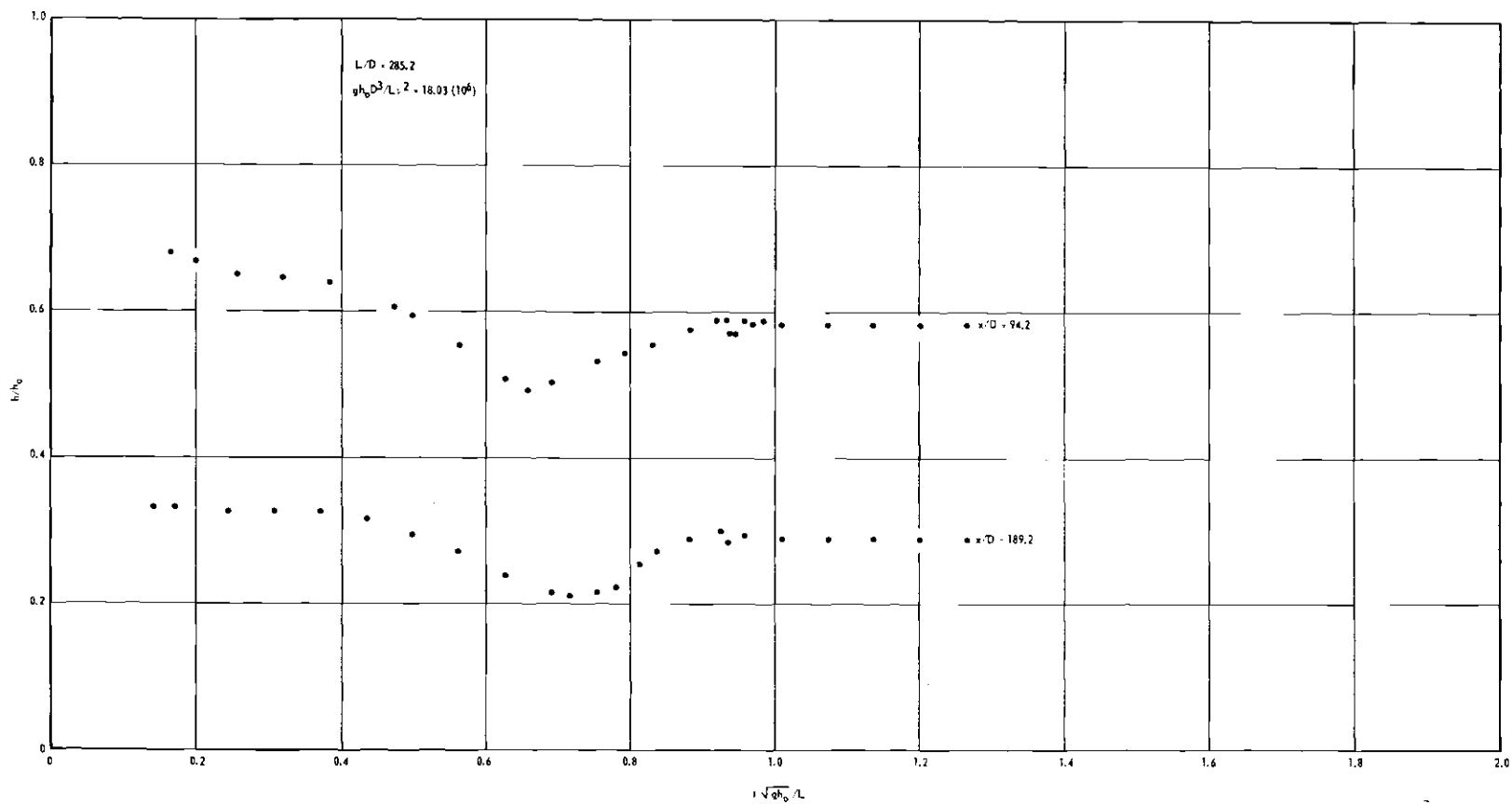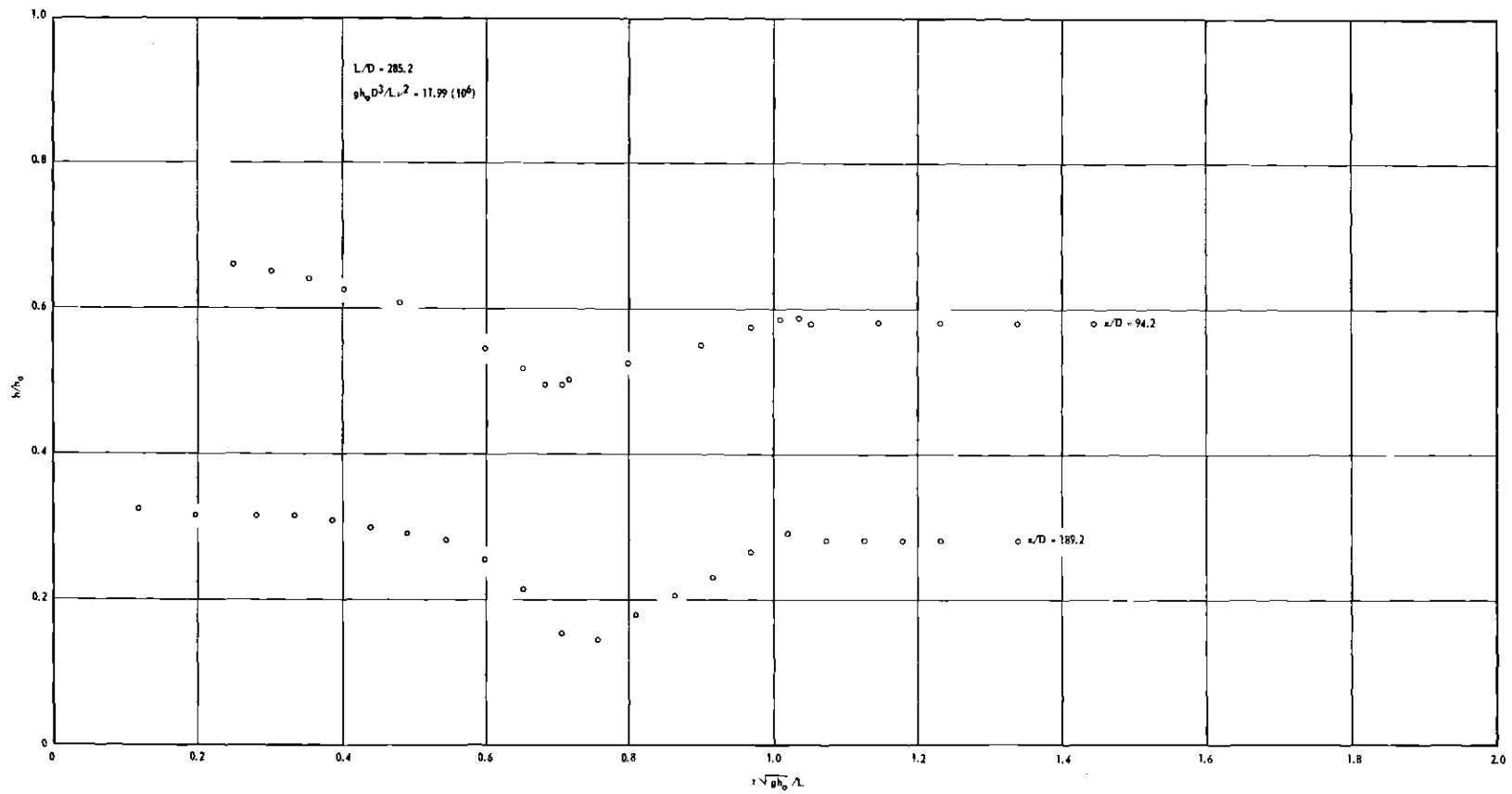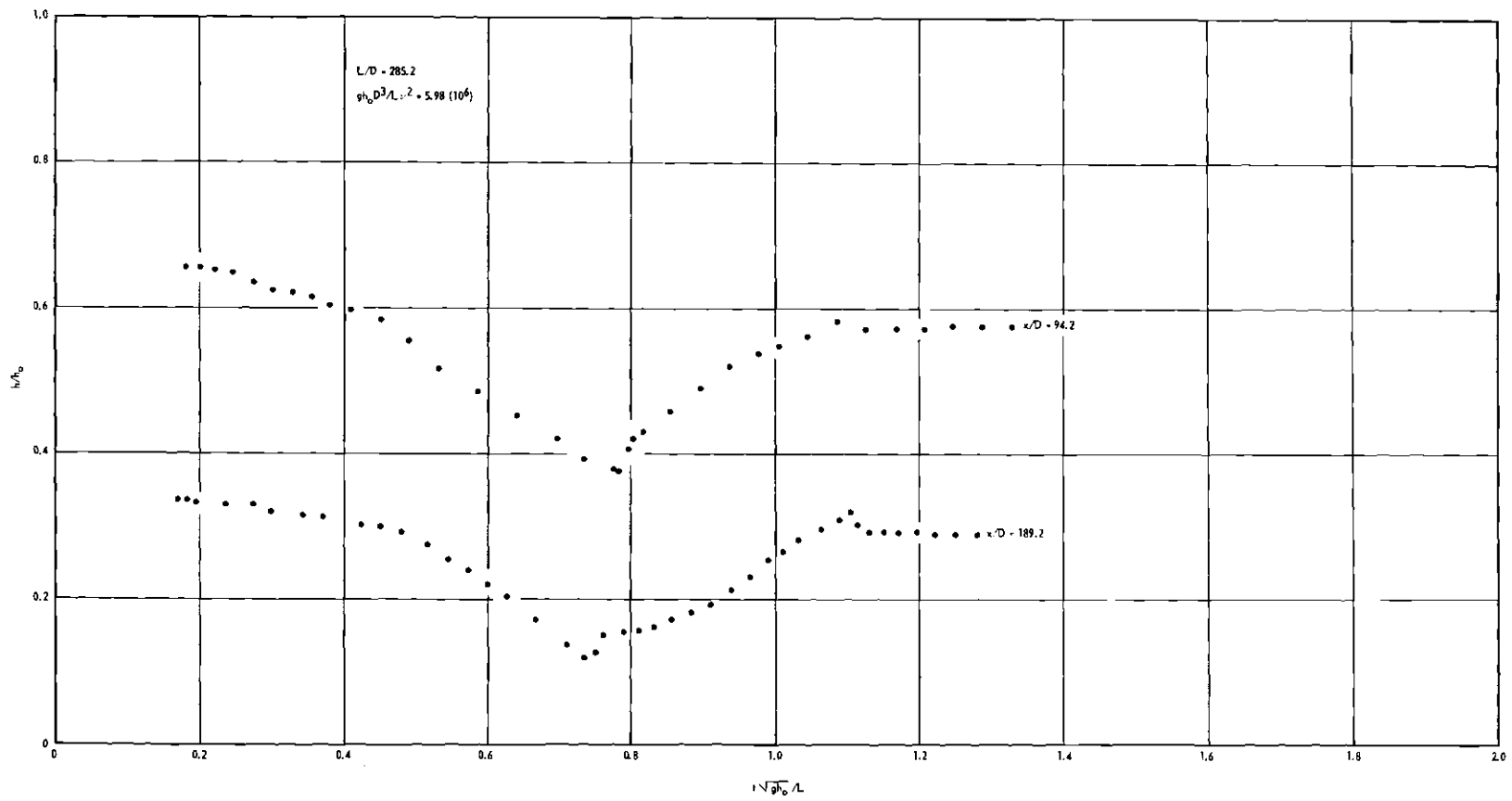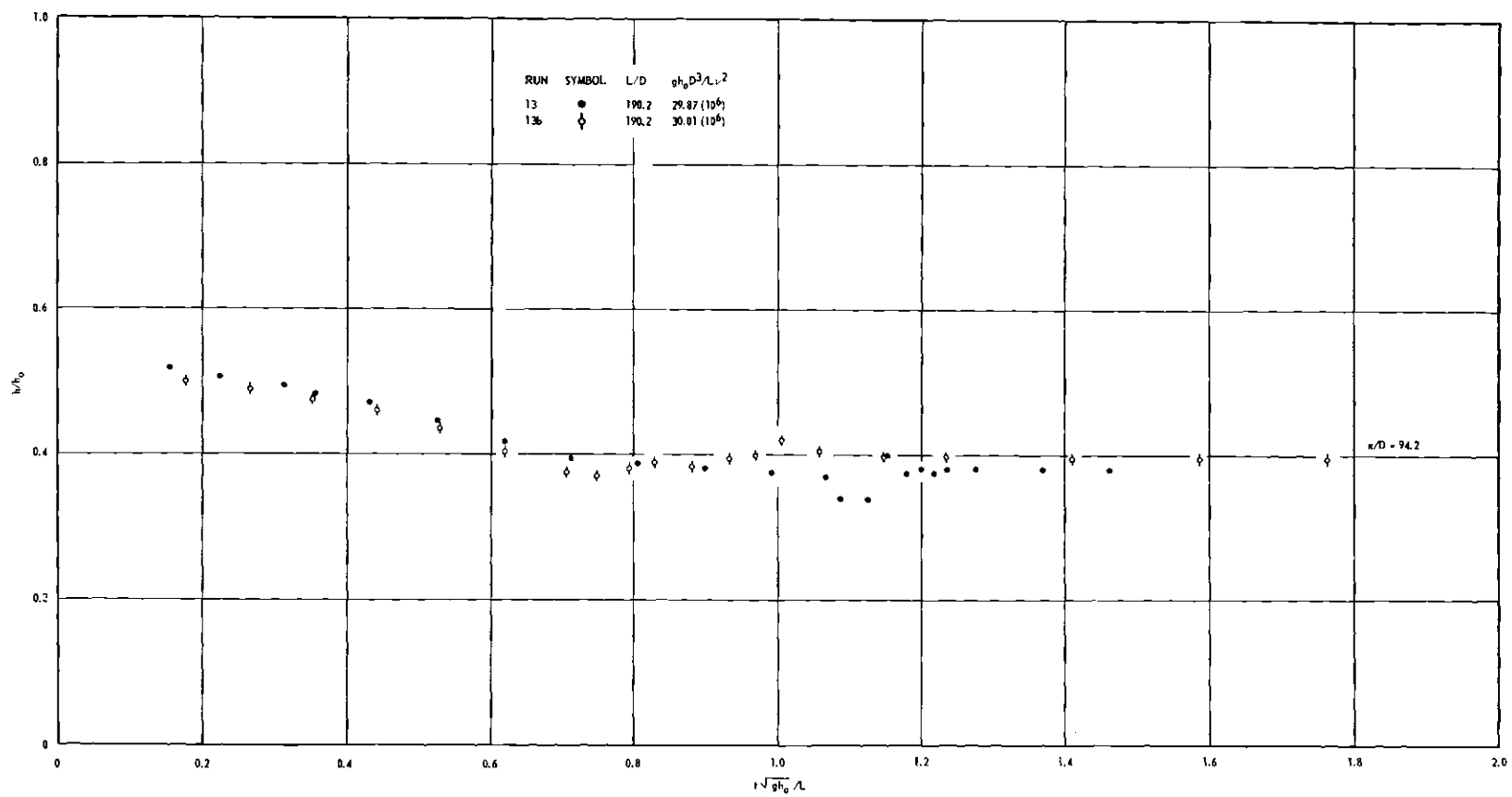
Figure 7A.   Pressure-time Data of Run 23.

Figure 8A.   Pressure-time Data of Run 22.

Figure 9A. Pressure-time Data of Run 21.

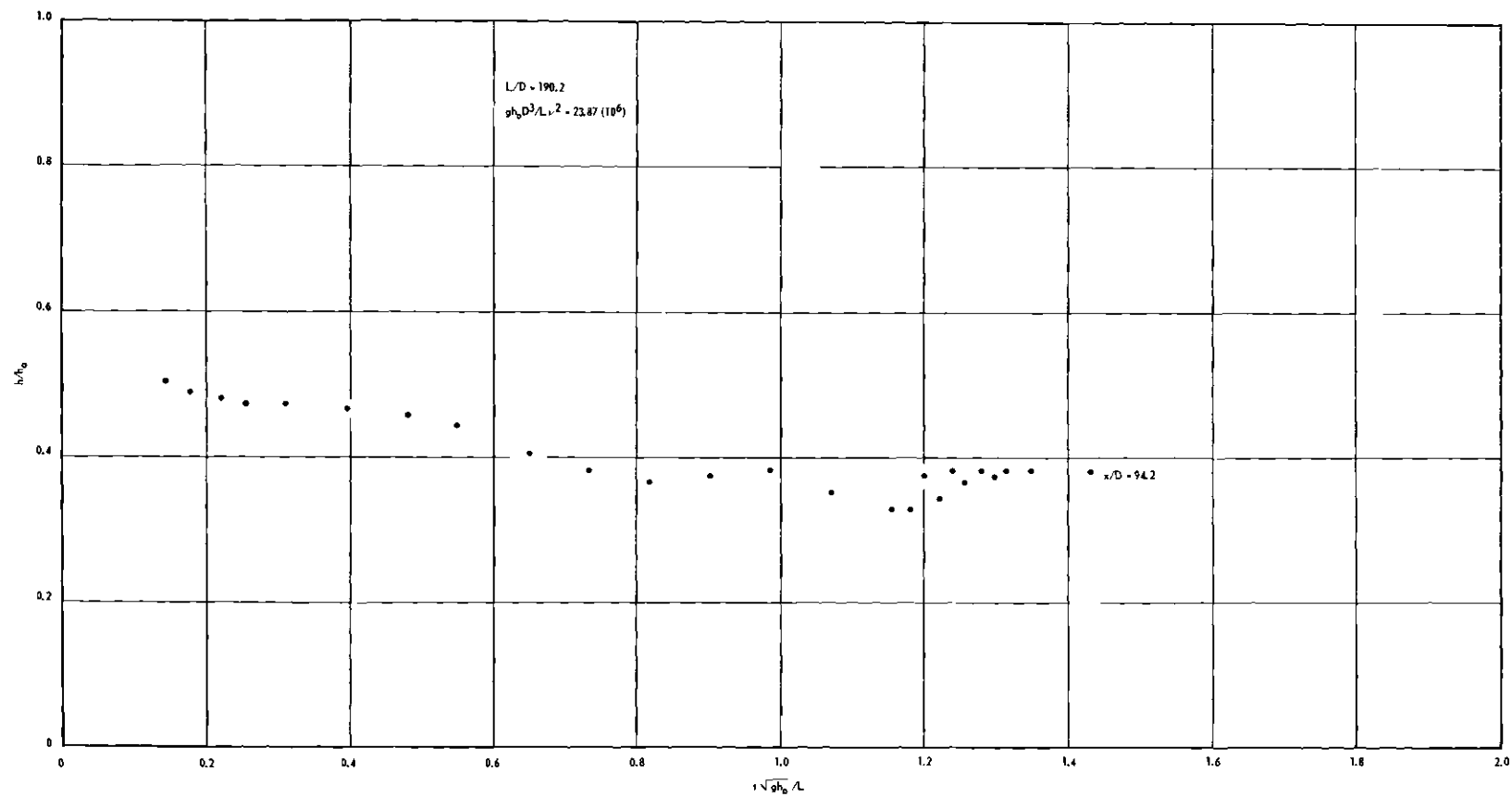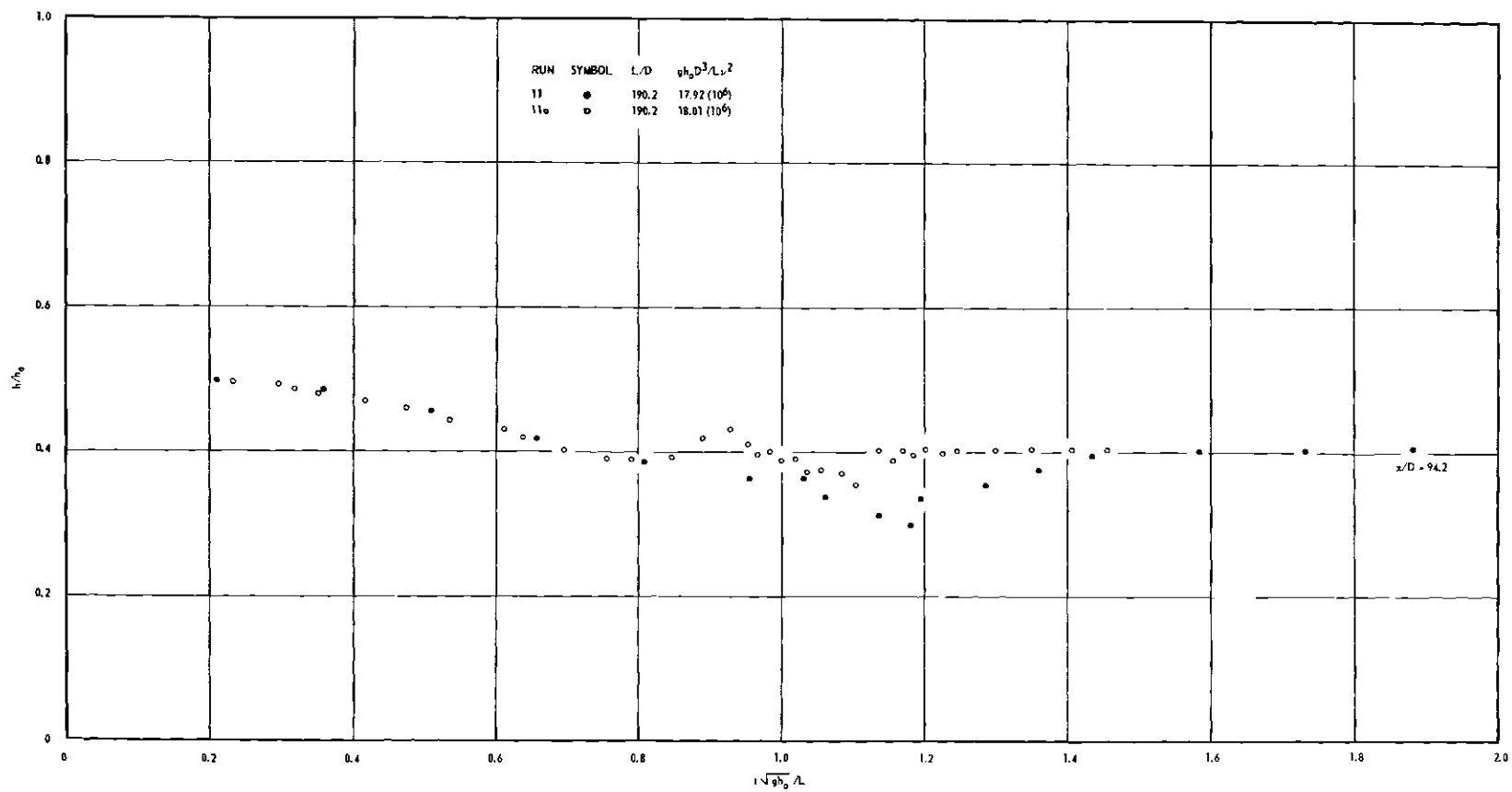Figure 10A.   Pressure-time Data of Run 20.

Figure 11A.   Pressure-time Data of Run 19.

Figure 12A. Pressure-time Data of Run 18.

Figure 13A.   Pressure-time Data of Run 17.

Figure 14A.   Pressure-time Data of Run 16a.

Figure 15A.   Pressure-time Data of Run 15.

Figure 16A.   Pressure-time Data of Run 13.

Figure 17A.   Pressure-time Data of Run 12.
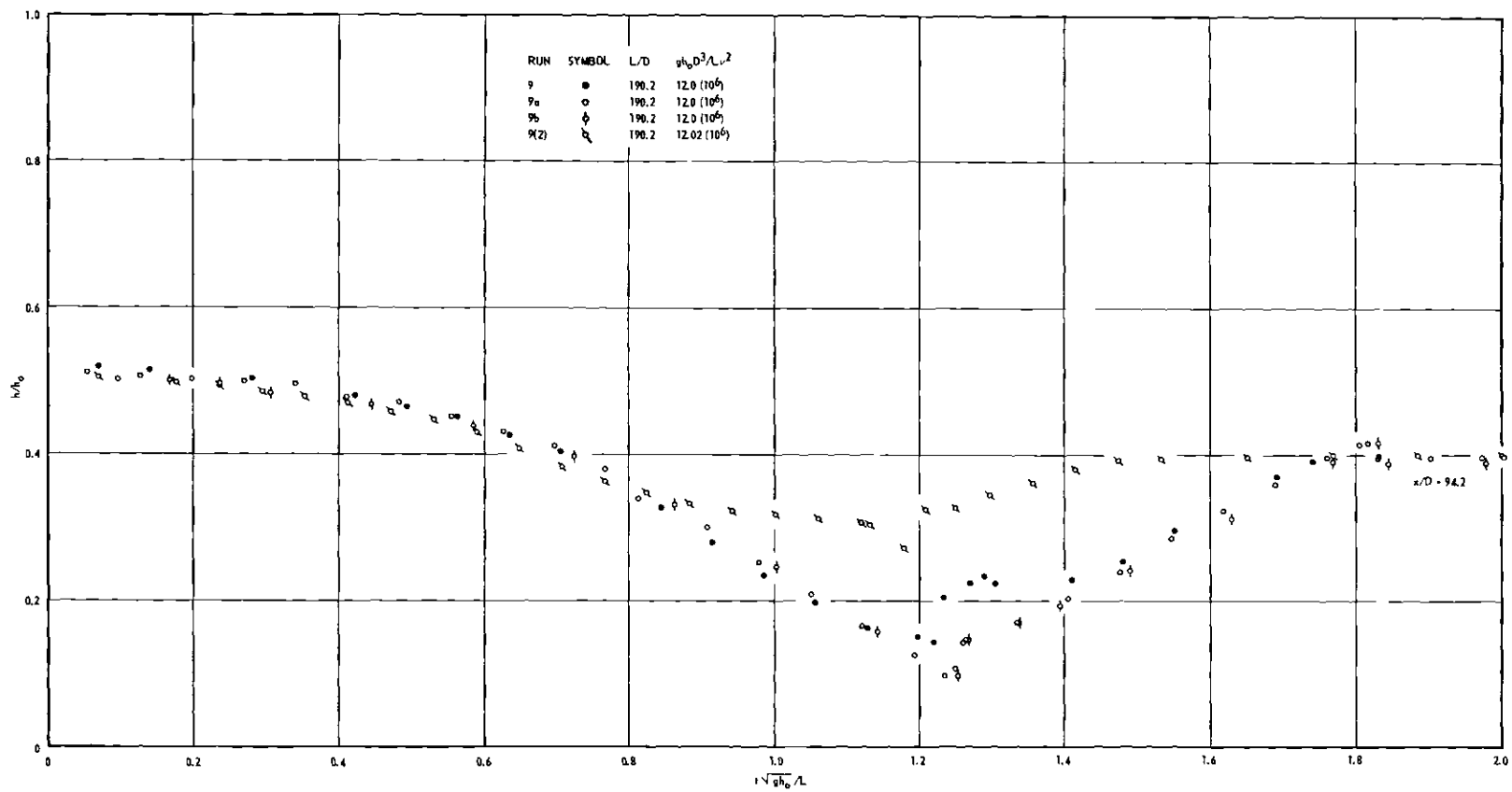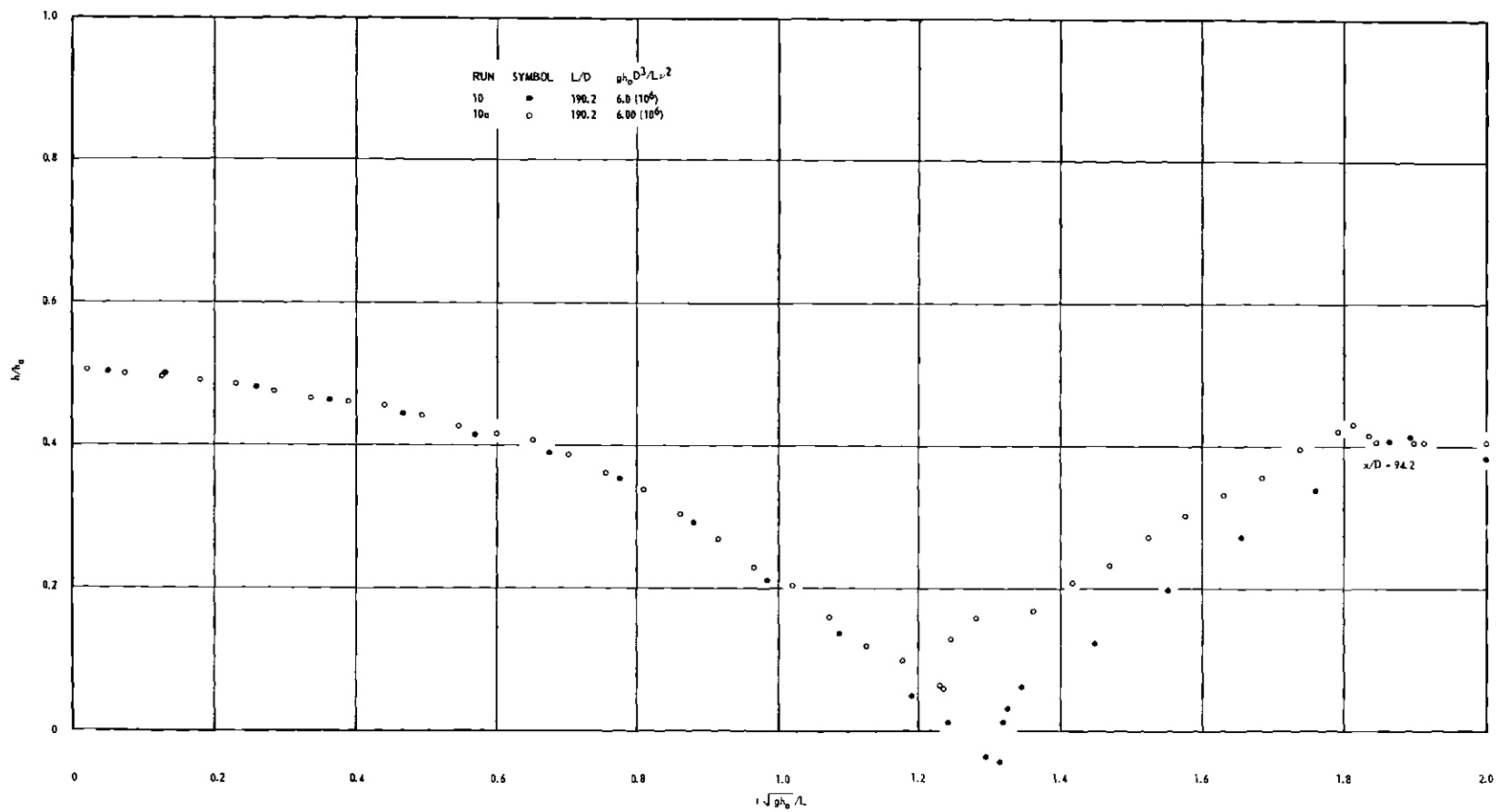
Figure 18A.   Pressure-time Data of Run 11.

Figure 19A.   Pressure-time Data of Run 9.

Figure 20A. Pressure-time Data of Run 10.